ОБЪЕДИНЕННЫЙ ИНСТИТУТ ЯДЕРНЫХ ИССЛЕДОВАНИЙ

Б2-2-89-791

ДЕПОНИРОВАННАЯ ПУБЛИКАЦИЯ

Дубна 1989

JOINT INSTITUTE FOR NUCLEAR RESEARCH

52-2-89-791

QCD ANALYSIS OF STRUCTURE FUNCTIONS

R. Lednicky

Abstract

The influence of various approximations and theoretical uncertienties on the determination of the QCD mass-scale parameter $\Lambda_{\overline{MS}}$, and, - on the QCD tests is studied with the help of the BCDMS hydrogen data. A small (negative) contribution of higher twists in the proton structure function $F_2(x,Q^2)$ is obtained in the region of moderate x and $Q^2 > 10\ GeV^2$, and, in agreement with theoretical models, it is well described in terms of one parameter $k^2 = 0.02\text{-}0.04\ GeV^2$ - the parton transverse momentum squared generated dynamically. This allows one to use the BCDMS data for a stringent QCD test and a reliable determination of $\Lambda_{\overline{MS}}$. The theoretical uncertienty in $\Lambda_{\overline{MS}}$ is dominated by the one due to the higher-order corrections.

23. 11. 89 г.

Dubna, 1989

ИНФОРМАЦИОННАЯ КАРТА

ы: Р.Ледницки

ние: КХД анализ структурных функций

убликации: депонированное сообщение ОИЯИ тематич.категория:

ключевые слова	указат. связи	ДЕСКРИПТОРЫ	тематич. рубрики
квантовая хромодинамика			
структурная функция			
анализ данных			

ширение названия:

рту составил: Р.Ледницки дата: 10.II.1989

L. Lednicky

ИНФОРМАЦИОННАЯ КАРТА

[ав]торы: Р.Ледницки

[На]звание: КХД анализ структурных функций

[ви]д публикации: депонированное сообщение ОИЯИ **тематич.категория:**

[№] п/п	ключевые слова	указат. связи	ДЕСКРИПТОРЫ	тематич. рубрики
I	квантовая хромодинамика			
2	структурная функция			
3	анализ данных			

расширение названия:

карту составил: Р.Ледницки дата: 10.II.1989

R. Lednicky

Р Е Ф Е Р А Т

С помощью водородных данных сотрудничества БЦДМС изучено влияние различных приближений и теоретических неопределенностей на определение масштабного параметра КХД и – на проверку КХД. В области средних x и $Q^2 > 10$ ГэВ^2 найден небольшой (отрицательны вклад высших твистов в протонную структурную функцию $F_2(x,Q^2)$, который, в соответствии с теоретическими моделями, хорошо описывае с помощью одного параметра $k^2 = 0{,}02 - 0{,}04$ ГэВ^2 – квадрата парто ного поперечного импульса, генерируемого за счет динамики. Это позволяет использовать данные БЦДМС для чувствительной проверки КХД и достоверного определения Λ. Преобладающий вклад в теоретичес неопределенность в Λ дают поправки от более высоких порядков теори

реферат составил: Р. Ледницки

L. Lednicky

ОИЯИ. Заказ 2244

1. Introduction

The pointlike and structureless nature of leptons has been extensively exploited to study the internal structure of the nucleon with the help of lepton-nucleon scattering. First the proton size was measured by electron scattering at the momentum transfer squared $Q^2 \sim 0.1\ GeV^2$ and, later on, the nucleon composite structure was discovered at SLAC at higher values of Q^2. The presence of pointlike constituents (partons = quarks) in the nucleon reveals itself as an approximate Bjorken scaling of the measured structure functions $F_k(x,Q^2)$. Thus, in the model of free collinear partons, the nucleon structure functions depend on the Bjorken scaling variable x only, e.g.

$$F_2^{ep}(x,Q^2) = x\cdot\sum_i e_i^2[q_i(x) + \bar{q}_i(x)],$$

$$F_2^{\nu p}(x,Q^2) = 2x\cdot[d(x) + s(x) + \bar{u}(x) + \bar{c}(x) + \ldots], \qquad (1)$$

where $q_i = d,\ u,\ s,\ c,\ b,\ \ldots$ represent the probability densities to find a quark of flavour i and electric charge e_i (in the units of the proton electric charge) carrying a fraction x of the proton momentum. The interpretation of partons as quarks is strongly supported by the fulfilment of Gross-Llewellyn Smith, Adler and Gottfried sum rules for the number of valence quarks in a nucleon ($3 = 3.0 \pm 0.2$), the difference between numbers of valence u- and d-quarks in a proton ($1 = 1.1 \pm 0.2$) and $e_u^2 - e_d^2$ ($1/3 = 0.24 \pm 0.11$), respectively (see, e.g. refs. [1,2]).

It follows from the momentum sum rule that only about half of the proton momentum is carried by quarks. The unprobed neutral partons are identified as gluons - carriers of the interaction between colour charges in quantum chromodynamics (QCD). This identification is supported by a weak (logarithmic) violation of Bjorken scaling, related in QCD to the gluon bremsstrahlung and quark-antiquark pair production. The predicted softening of the parton x-distributions with Q^2 agrees with the character of scaling violations observed experimentally, though, there is some discrepancy between the most precise high energy data of EMC and BCDMS [2-4].

Since the QCD effective coupling $\alpha_s(Q^2)$ logarithmically vanishes with Q^2 (asymptotic freedom) the scaling violations should do the same. Present deep-inelastic scattering data are not accurate enough to check running of α_s. However, the precission and the Q^2-range of recent BCDMS data [5-11] appear to be sufficient to quantitatively check the QCD predictions for scaling violations, to reliably determine α_s (or QCD mass-scale parameter Λ), and, to check consistency of the predictions for various targets (same α_s). These data have also important implications for predicting W and Z production rates on $\bar{p}p$ colliders and thus placing limits on the number of light neutrinos and, possibly, on the mass of the top quark [12].

In this paper we use the BCDMS hydrogen data [8,9] to study the influence of various approximations and theoretical uncertienties on the determination of the QCD mass-scale parameter Λ and - on the QCD tests. Basic formulae of perturbative QCD for deep-inelastic scattering, including α_s^2-corrections to the longitudinal structure function, are reviewed in Section 2. In Section 3 we discuss various methods for solving the QCD evolution equations, in particular - the simple and convenient method of Jacobi polynomial reconstruction of structure functions. In this Section we also study the uncertienties of QCD fits due to finite reconstruction accuracy and limited flexibility of parton parametrizations, and, discuss the problem of QCD tests. The uncertienties due to various preasymptotic corrections to the perturbative QCD predictions, including higher-order-, flavour threshold- and higher twist-corrections, are discussed in Section 4. The conclusions are summarized in Section 5.

2. Perturbative QCD predictions for inclusive leptoproduction

2.1 Cross sections and structure functions

The cross sections of deep-inelastic inclusive lepton scattering on unpolarized nucleons, $l^{\pm}\ N \rightarrow l^{\pm}\ X$ and $\nu_l/\bar{\nu}_l\ N \rightarrow l^-/l^+\ X$, in the one-boson exchange approximation, are expressed through the nucleon structure functions $F_k(x,Q^2)$ in the form ($m_l^2 \ll Q^2 \ll m_{W,Z}^2$):

$$\frac{d\sigma^{\mu,e}}{dx dQ^2} = \frac{4\pi\alpha^2}{x\cdot Q^4}\left[xy^2F_1(x,Q^2)+\left(1-y-\frac{Mxy}{2E}\right)F_2(x,Q^2)\right], \qquad (2)$$

$$\frac{d\sigma^{\nu/\bar\nu}}{dx dy} = \frac{G^2ME}{\pi}\left[xy^2F_1^{\nu/\bar\nu}(x,Q^2)+\left(1-y-\frac{Mxy}{2E}\right)F_2^{\nu/\bar\nu}(x,Q^2)\pm \right.$$

$$\left.\pm\left(1-\frac{y}{2}\right)xyF_3^{\nu/\bar\nu}(x,Q^2)\right], \qquad (3)$$

where $\alpha \simeq 1/137$, $G \simeq 1.166\cdot10^{-5}$ GeV^{-2}, $x = \frac{Q^2}{2M\nu}$ is the Bjorken scaling variable, M is the nucleon mass, $y = \nu/E$, $\nu = E-E'$, E and E' are the energies of the initial and the scattered lepton. To exctract these cross sections from the measured ones the radiative corrections should be applied. They are known quite precisely. E.g., for the charged lepton scattering, in the region of large y (small x) covered by BCDMS data, they introduce an uncertienty in $F_2(x,Q^2)$ less than 1%, otherwise, the uncertienty is much smaller [13].

In the parton model approximation, the Callan-Gross relation $F_2= 2xF_1$ is valid at $Q^2 \gg M^2$ as a consequence of vanishing coupling of longitudinally polarized photons to quarks. The violation of this relation is measured by the longitudinal structure function

$$F_L(x,Q^2) = (1+\varepsilon)F_2(x,Q^2) - 2xF_1(x,Q^2), \qquad \varepsilon = 4M^2x^2/Q^2, \qquad (4)$$

or, by the ratio of the cross sections of the absorption of longitudinally and transversally polarized photons on a nucleon target:

$$R(x,Q^2) = \frac{\sigma_L}{\sigma_T} = \frac{F_L}{2xF_1} = \frac{F_L}{(1+\varepsilon)F_2-F_L}\ . \qquad (5)$$

In terms of the structure functions $F_2(x,Q^2)$ and $R(x,Q^2)$, the cross section in eq. (2) can be rewritten in the form

$$\frac{d\sigma^{\mu,e}}{dx dQ^2} = \frac{4\pi\alpha^2}{x\cdot Q^4}\left[1-y-\frac{1}{4}\varepsilon y^2+\frac{1}{2}y^2\frac{1+\varepsilon}{1+R(x,Q^2)}\right]\cdot F_2(x,Q^2). \qquad (6)$$

It may be seen that the cross section is sensitive to the structure function $R(x,Q^2)$ only at sufficiently large y-values.

2.2 Q^2-evolution of structure functions

According to the QCD factorization theorem, the structure functions are given as the convolution of quark and gluon densities q_i and G with the coefficient functions C_k (which are proportional to the corresponding cross sections of the hard process - the absorption of the intermediate boson by a parton):

$$f_k(x,Q^2) = \int_x^1 \frac{dy}{y} \left[C_k^{NS}(\frac{x}{y},Q^2)A^{NS}(y,Q^2) + C_k^{SI}(\frac{x}{y},Q^2)A^{SI}(y,Q^2) + \right.$$
$$\left. + C_k^G(\frac{x}{y},Q^2)A^G(y,Q^2)\right], \tag{7}$$

where $f_2 = F_2/x$, $f_1 = \frac{1}{2}F_1$ and $f_3 = F_3$. The functions $A^G \propto G$, A^{SI} and A^{NS} are certain flavour singlet and nonsinglet combinations of the parton densities. E.g., in the case of charged lepton scattering, assuming $f/2$ doublets of zero mass quarks,

$$A^G = \frac{5}{18}G, \quad A^{SI} = \frac{5}{18}\sum_{i=1}^{f}(q_i+\bar{q}_i), \quad A^{NS} = \frac{1}{6}(u-d+\bar{u}-\bar{d}+c-s+\bar{c}-\bar{s}+..). \tag{8}$$

The coefficients $\frac{5}{18}$ and $\frac{1}{6}$ are nothing else but half the sum and the difference of the electric charges squared of the quarks in a doublet, respectively.

It should be noted that both the coefficient functions and parton densities are dependent on the renormalization (factorization) scheme and on the renormalization scale parameter μ (the choice $\mu = Q$, assumed in eq. (7), introduces Q^2-dependence of the parton densities). Of course, their convolution, being a physical quantity, must be independent on the renormalization procedure provided both the factors are calculated in the same scheme. In the following, we use the results obtained in the modified minimal subtraction ($\overline{MS}$) scheme [14]. In particular, the parton densities defined in this scheme satisfy the usual momentum sum rule:

$$\langle x_q\rangle + \langle x_G\rangle = \int_0^1 dx\cdot x\cdot\{\sum_{i=1}^{f} [q_i(x,Q^2)+\bar{q}_i(x,Q^2)] + G(x,Q^2)\} = 1. \quad (9)$$

The parton densities are often defined in a different way [15,16] by demanding $F_2^{\nu N}(x,Q^2)$ to maintain the same form as in the parton model. Such a modification of the scheme slightly simplifies the calculation of this particular structure function, but has no preference in other cases.

The coefficient functions can be expanded in powers of the running coupling constant $\alpha_s(Q^2)$:

$$C_k(x,Q^2) = C_k^{(0)}(x) + \frac{\alpha_s(Q^2)}{2\pi} C_k^{(1)}(x) + [\frac{\alpha_s(Q^2)}{2\pi}]^2 C_k^{(2)}(x) + .., \quad (10)$$

where $C_k^{SI(0)}(x) = C_k^{NS(0)}(x) = \delta(x-1)$, $C_k^{G(0)}(x) = 0$ and $C_k^{SI(1)}(x) = C_k^{NS(1)}(x)$, $k = 1,2,3$. The functions $C_k^{(i)}(x)$ are Q^2 independent in the limit of massless quarks. At $\alpha_s \to 0$, eq. (7) yields the parton model result, e.g., eqs. (1).

The effective coupling $\alpha_s(Q^2)$ obeys the QCD beta function renormalization group equation

$$4\pi d(\frac{1}{\alpha_s}) = [\beta_0 + \frac{\alpha_s}{4\pi}\beta_1 + (\frac{\alpha_s}{4\pi})^2\beta_2 + ..] d\ln Q^2, \quad (11)$$

where β_i are the beta function expansion coefficients, e.g.

$$\beta_0 = 11 - \frac{2}{3}f, \quad \beta_1 = 102 - \frac{38}{3}f, \quad \beta_2 = \frac{2857}{2} - \frac{5033}{18}f + \frac{325}{54}f^2, \quad (12)$$

f is the number of active flavours. The coefficients β_0 and β_1 are independent on the renormalization scheme, β_2 in eq. (12) corresponds to the $\overline{\mathrm{MS}}$ scheme [17]. Eq. (11), in the leading order (LO) of α_s on the rhs yields

$$\alpha_s^{(0)}(Q^2) = \frac{4\pi}{\beta_0 \ln(Q^2/\Lambda^2)}, \quad (13)$$

and, in the next-to-leading order (NLO), $\alpha_s = \alpha_s^{(1)}(Q^2)$ is given by the implicit equation [18]:

$$\ln\frac{Q^2}{\Lambda^2} = \frac{4\pi}{\beta_0\alpha_s} - \frac{\beta_1}{\beta_0^2}\ln[(\frac{4\pi}{\beta_0\alpha_s} + \frac{\beta_1}{\beta_0^2})/C], \quad (14)$$

where Λ is an unknown integration constant (QCD mass scale parameter) to be determined from experiment. The constant C on the rhs of eq. (14) indicates that the definition of the scale Λ is merely a matter of convention. The commonly used choice is $C = 1$ [14,19], though other choices are sometimes prefered, e.g., $C = \beta_1/\beta_0^2$ [18] or $C = 2\beta_0$ [20]. The scales at different C-values are related by:

$$\Lambda(C') = \Lambda(C)\cdot(C'/C)^{\beta_1/2\beta_0^2}.$$

The solution of eq. (11) can be represented as a series of the terms $ln^m[C\cdot ln(Q^2/\Lambda^2)]/ln^n(Q^2/\Lambda^2)$, $m = 0,1,..n$. In particular, at $C = 1$ we have in the NLO:

$$\alpha_s^{(1)}(Q^2) = \alpha_s^{(0)}(Q^2)/[1 + \frac{\alpha_s^{(0)}(Q^2)}{4\pi}\frac{\beta_1}{\beta_0}ln ln\frac{Q^2}{\Lambda^2}] \cong \tag{14'}$$

$$\cong \alpha_s^{(0)}(Q^2)\cdot[1 - \frac{\alpha_s^{(0)}(Q^2)}{4\pi}\frac{\beta_1}{\beta_0}ln ln\frac{Q^2}{\Lambda^2}], \tag{14''}$$

and, in yet the higher-order:

$$\alpha_s^{(2)}(Q^2) = \alpha_s^{(0)}(Q^2)/\{1 + \frac{\alpha_s^{(0)}(Q^2)}{4\pi}\frac{\beta_1}{\beta_0}ln ln\frac{Q^2}{\Lambda^2} + [\frac{\alpha_s^{(0)}(Q^2)}{4\pi}]^2\,[(\frac{\beta_1}{\beta_0})^2(1 + ln ln\frac{Q^2}{\Lambda^2}) - \frac{\beta_2}{\beta_0}]\}, \tag{15}$$

In the BCDMS Q^2-range and at $\Lambda \approx 200$ MeV eqs. (14') and (14''), as compared with the equally valid NLO expression (14), give the α_s-values higher by 3% and lower by 2%, respectively. Eqs. (14'), (14'') and (14) yield the same α_s as the second order eq. (15) at the Λ-values lower by 15 MeV and higher by 25 MeV and 10 MeV, respectively.

The Q^2 dependence of the parton densities $A^i(x,Q^2)$ is governed by solutions of the generalized Altarelli-Parisi-Lipatov evolution equations:

$$\frac{\partial A_{\pm}^{NS}(x,Q^2)}{\partial lnQ^2} = \int_x^1 \frac{dy}{y} A_{\pm}^{NS}(y,Q^2)P_{\pm}(\frac{x}{y},Q^2),$$

$$\frac{\partial A^{SI}(x,Q^2)}{\partial lnQ^2} = \int_x^1 \frac{dy}{y} [A^{SI}(y,Q^2)P_{qq}(\frac{x}{y},Q^2) + A^G(y,Q^2)P_{qG}(\frac{x}{y},Q^2)],$$

$$\frac{\partial A^G(x,Q^2)}{\partial lnQ^2} = \int_x^1 \frac{dy}{y} [A^{SI}(y,Q^2)P_{Gq}(\frac{x}{y},Q^2) + A^G(y,Q^2)P_{GG}(\frac{x}{y},Q^2)], \qquad (16)$$

where the splitting functions P_{ij} are the probabilities of $j \to i$ (P_{qG} is sometimes redefined by $P_{qG} \to 2fP_{qG}$). The index + (-) in the NS-equation denotes the evolution of a crossing even (odd) combination of parton densities, i.e. of a one containing $q_i+\bar{q}_i$ ($q_i-\bar{q}_i$).

The Q^2 dependence of the splitting functions is determined by the expansion in powers of the running coupling constant $\alpha_s(Q^2)$:

$$P_{ij}(x,Q^2) = \frac{\alpha_s(Q^2)}{2\pi} P_{ij}^{(0)}(x) + [\frac{\alpha_s(Q^2)}{2\pi}]^2 P_{ij}^{(1)}(x) + \dots \quad . \qquad (17)$$

Note that $P_+^{(l)} \neq P_-^{(l)}$ for $l \geqslant 1$ due to the $q \leftrightarrow \bar{q}$ mixing terms which arise in the next-to-leading and higher orders. Both the coefficient and the splitting functions have been calculated up to the next-to-leading order (see reviews [21,22], references therein and refs. [23,24]).

2.3 *Analytical solutions of evolution equations in moment representation*

The Mellin transformation

$$f(n) = \int_0^1 dx \cdot x^{n-1} f(x) \qquad (18)$$

allows one to transform the convolution integrals into simple multiplications. Thus, e.g., eq. (7) becomes

$$f_k(n,Q^2) = C_k^{NS}(n,Q^2)A^{NS}(n,Q^2) + C_k^{SI}(n,Q^2)A^{SI}(n,Q^2) + \\ + C_k^G(n,Q^2)A^G(n,Q^2). \qquad (7')$$

By tradition, the expansion of $C_k(n,Q^2)$ in powers of α_s is defined differently than in eq. (10):

$$C_k(n,Q^2) = B^{(0)}_{k,n} + \frac{\alpha_s(Q^2)}{4\pi} B^{(1)}_{k,n} + [\frac{\alpha_s(Q^2)}{4\pi}]^2 B^{(2)}_{k,n} + \ldots, \qquad (10')$$

i.e. $B^{(l)}_{k,n} = 2^l C^{(l)}_k(n)$.

The solution of the Mellin transformed evolution equations is straightforward:

$$A^{NS}_\pm(n,Q^2) = \phi^{NS}_\pm(n,Q^2,Q_0^2)A^{NS}_\pm(n,Q_0^2),$$
$$A^{SI}(n,Q^2) = \phi_{qq}(n,Q^2,Q_0^2)A^{SI}(n,Q_0^2) + \phi_{qG}(n,Q^2,Q_0^2)A^G(n,Q_0^2),$$
$$A^G(n,Q^2) = \phi_{Gq}(n,Q^2,Q_0^2)A^{SI}(n,Q_0^2) + \phi_{GG}(n,Q^2,Q_0^2)A^G(n,Q_0^2). \qquad (19)$$

Here the initial moments $A^i(n,Q^2)$ at some reference point Q_0^2 are not predicted by perturbative QCD. The ϕ-functions are determined by the Mellin transform of the splitting functions. Introducing

$$\gamma_{ij}(n,Q^2) = -2P_{ij}(n,Q^2) = \frac{\alpha_s}{4\pi}\gamma^{(0)}_{ij}(n) + (\frac{\alpha_s}{4\pi})^2\gamma^{(1)}_{ij}(n) + \ldots, \qquad (17')$$

then, e.g., the nonsinglet ϕ-function reads as follows:

$$\phi^{NS}_\pm(n,Q^2,Q_0^2) = [\frac{\alpha_s(Q^2)}{\alpha_s(Q_0^2)}]^{\gamma^{(0)}_\pm(n)/2\beta_0} H^{NS}_\pm(n,Q^2,Q_0^2),$$
$$H^{NS}_\pm(n,Q^2,Q_0^2) = 1 + \frac{1}{4\pi}[\alpha_s(Q^2)-\alpha_s(Q_0^2)]\cdot Z^{NS}_\pm(n),$$
$$Z^{NS}_\pm(n) = [\gamma^{(1)}_\pm(n) - \gamma^{(0)}_\pm(n)\beta_1/\beta_0]/2\beta_0. \qquad (20)$$

Similar expressions for the singlet ϕ-functions can be read out from eqs. (2.138) - (2.143) of the review [25]. The solutions of the evolution equations should not depend on the reference point $Q_0{}^2$. The ϕ-function in eq. (20) fulfils this requirement only in the NLO in $\alpha_s(Q_0{}^2)$. Therefore, it becomes unvalid if $Q_0{}^2$ has been chosen too low. The $Q_0{}^2$-independence in the low-$Q_0{}^2$ region can be recovered by solving the NLO Mellin transformed evolution equations exactly, i.e. replacing the H-function in eq. (20) by [26]:

$$H^{NS}_{\pm}(n,Q^2,Q_0^2) = \left[\frac{1 + \frac{\beta_1}{\beta_0}\frac{\alpha_s(Q^2)}{4\pi}}{1 + \frac{\beta_1}{\beta_0}\frac{\alpha_s(Q_0^2)}{4\pi}} \right]^{\frac{\beta_0}{\beta_1}Z^{NS}_{\pm}(n)} . \qquad (20')$$

In fact, the QCD predictions in terms of the Mellin moments have been originally obtained with the help of the Wilson operator product expansion (OPE); $\gamma_{\pm}(n,Q^2)$ at even/odd n are just the anomalous dimensions of the spin-n nonsinglet operators. Both $C_k(n,Q^2)$ and $\gamma(n,Q^2)$ are known up to the next-to-leading order. In particular, the anomalous dimensions have been calculated in [27] and represented in a simple analytical form in [28,29]. Note that the gluon-gluon anomalous dimension of refs. [27,28] slightly differes from the generally accepted result of refs. [29,30].

Recall that the anomalous dimensions beyond the leading order predict only even/odd moments of the crossing even/odd structure functions [31]. To find out the evolution of the moments at any n, an analytical continuation should be performed for even and odd n separately. As a result, the relevant moments defined in eq. (17') are related to the OPE anomalous dimensions γ_n^{NS} and γ_n^{SI} by the following expressions:

$$\gamma_{\pm}^{(l)}(n) = \gamma_n^{NS(l)} + \eta_{\pm}(n)\Delta\gamma_n^{NS(l)},$$

$$\gamma^{(l)}(n) = \gamma_n^{SI(l)} + \eta_{+}(n)\Delta\gamma_n^{SI(l)},$$

$$\eta_{\pm}(n) = \pm 1-(-1)^n, \qquad (21)$$

where $\Delta\gamma_n^{(0)} = 0$, and, the corrections $\Delta\gamma_n^{(1)}$ are known to be quite small and vanishing very fast with n ($\Delta\gamma_n^{NS} \propto 1/n^6$) [31]. The corrections in the crossing even/odd case can be simply taken into account by the following replacements in the OPE anomalous dimensions [26,32]:

$$(-1)^n \;\to\; \pm 1,$$

$$S_2'(\tfrac{1}{2}n) \;\to\; (-1)^n\{\pm S_2'(\tfrac{1}{2}n) + \eta_{\pm}(n)[-2S_2(n) + \zeta(2)]\},$$

$$S_3'(\tfrac{1}{2}n) \;\to\; (-1)^n\{\pm S_3'(\tfrac{1}{2}n) + \eta_{\pm}(n)[-4S_3(n) + 3\,\zeta(3)]\},$$

$$\tilde{S}(n) \;\to\; (-1)^n[\pm\tilde{S}(n) + \eta_{\pm}(n)\,\tfrac{5}{8}\,\zeta(3)], \qquad (22)$$

where the series $S_m(n)$ and the alternate serieses $S_m(\frac{1}{2}n)$, $\tilde{S}(n)$ are defined in [28] and $\zeta(z)$ is the Riemann zeta function, $\zeta(2) = \pi^2/6$, $\zeta(3) \cong 1.20205\ 69031\ 59594$.

2.4 NLO calculation of longitudinal structure function

The QCD prediction for the longitudinal structure function, defined in eq. (4), is given, at $Q^2 \gg M^2$, by eq. (7), where

$$f_L(x,Q^2) = F_L(x,Q^2)/x, \qquad C_L(x,Q^2) = C_2(x,Q^2) - C_1(x,Q^2).$$

Since $C_L^{(0)}(x) = 0$, due to the helicity conservation, the leading order QCD prediction for $F_L(x,Q^2)$ is proportional to α_s:

$$F_L(x,Q^2) = \frac{\alpha_s(Q^2)}{2\pi} x\int_x^1 \frac{dy}{y} [C_L^{NS(1)}(\frac{x}{y})\frac{F_2(y,Q^2)}{y} + C_L^{G(1)}(\frac{x}{y})A^G(y,Q^2)]. \quad (23)$$

Here

$$C_L^{NS(1)}(x) = C_L^{SI(1)}(x) = \frac{8}{3}x, \quad C_L^{G(1)}(x) = 4fx(1-x), \quad (24)$$

being the LO quantities, are independent on the renormalization scheme (eq. (23) is sometimes confusingly called as the NLO one, though it is understood that it should be used with α_s and the parton densities calculated in the LO [25]). To get the NLO QCD predictions, the α_s^2-terms $C_L^{(2)}(x)$ in the coefficient functions $C_L(x,Q^2)$ are needed. Analytic results for $C_L^{NS(2)}(x)$ and $C_L^{SI(2)}(x)$ have been obtained in refs. [23,24]. The Mellin moments of the α_s^2-terms were calculated partly numerically in the nonsinglet case [23] and, recently, in an analytical form for all the nonsinglet-, singlet- quark and gluon coefficient functions [33]. The results contain the alternate serieses $K_m(n) = S_m(n)-S'_m(\frac{1}{2}n)/2^{m-1}$ and $Q(n) = -\tilde{S}(n)$ which should be continued from even to odd n by the replacements (22) for the crossing even case (see eqs. (43) of ref. [33]). The coefficients $B_{L,n}^{i(2)}$ in the expansion (10') are given in eqs. (35), (38) and (41) of ref. [33] through the ratios $R_{L,n}^{(2)} = B_{L,n}^{(2)}/B_{L,n}^{(1)}$, where $B_{L,n}^{(1)} = 2C_L^{(1)}(n)$,

$$B_{L,n}^{NS(1)} = B_{L,n}^{SI(1)} = \frac{16/3}{n+1}, \quad B_{L,n}^{G(1)} = \frac{8f}{(n+1)(n+2)} . \quad (25)$$

We can invert the Mellin moments of a longitudinal structure function, given by eq. (7'), with the help of the methods discussed in Sect. 3.1, or, neglect a small difference between the NS and SI values of $R^{(2)}_{L,n}$, which is essential (>10%) only at small n ($n \leqslant 3$), i.e. only at small x, and write $F_L(x,Q^2)$ in the form similar to eq. (23) (see also ref. [34]):

$$F_L(x,Q^2) = \frac{\alpha_s(Q^2)}{2\pi} x\int_x^1 \frac{dy}{y} \{C_L^{NS(1)}(\tfrac{x}{y})[1+\frac{\alpha_s(Q^2)}{4\pi} R^q(\tfrac{x}{y})]\frac{F_2(y,Q^2)}{y} + $$
$$+ C_L^{G(1)}(\tfrac{x}{y})[1+\frac{\alpha_s(Q^2)}{4\pi} R^G(\tfrac{x}{y})]A^G(y,Q^2)\}, \qquad (26)$$

where the functions $R^q(x)$ and $R^G(x)$ are defined by the relations:

$$B^{NS(1)}_{L,n}(R^{NS(2)}_{L,n} - B^{NS(1)}_{2,n}) = 2\int_0^1 dx\cdot x^{n-1} C_L^{NS(1)}(x)R^q(x), \qquad (27)$$

$$B^{G(1)}_{L,n}R^{G(2)}_{L,n} - B^{NS(1)}_{L,n}B^{G(1)}_{2,n} = 2\int_0^1 dx\cdot x^{n-1} C_L^{G(1)}(x)R^G(x). \qquad (28)$$

The approximation $R^{SI}_{L,n} = R^{NS}_{L,n}$, assumed in eq. (26), leads to ~ 4% overestimation of $F_L(x,Q^2)$ in the lowest BCDMS x,Q^2-bins. The overestimation becomes less than 1% for $x > 0.3$. At $f = 4$, the following simple but sufficiently accurate parametrizations for the R^i-functions can be used:

$$R^q(x) = 36.5x^2, \qquad R^G(x) = 240.9x^5. \qquad (29)$$

They satisfy eqs. (27) and (28) with an accuracy better than 1% ($2 < n < 11$) and 2% ($3 < n < 11$), respectively, i.e. - underestimate $F_L(x,Q^2)$ by 3-7% for $x = 0.07$-0.14, and, overestimate it by 4-11% for $x = 0.35$-0.75.

The $\alpha_s{}^2$-corrections to the longitudinal coefficient functions are quite large. Thus the neglect in refs. [8,9,11] of the correction terms in square brackets in eq. (26) underestimates $F_L(x,Q^2)$ in the NLO by about 30%. At the same time, they are compensated, to a large extent, by the NLO corrections to $\alpha_s(Q^2)$ and to the parton distributions. As may be seen from fig. 1 the net NLO correction remains positive but it is less than 10% in major part of the BCDMS kinematic region. The uncertienty in F_L due to the higher-order corrections is expected to be of similar size (see Section 4.1).

3. Calculation and fit procedures

3.1 Calculating QCD predictions for structure functions. Survey of methods.

The comparison of the theoretical and the experimental moments of the structure functions is technically very easy. However, due to the necessity of an interpolation of the data into the unmeasured regions $x \to 0,\ 1$, such a comparison is commonly considered to be less reliable than a direct QCD analysis of the measured structure functions. Thus the evolution equations (16), as well as the convolution (7), effectively require only an interpolation to $x = 1$ which introduces a negligable uncertienty (due to rapidly vanishing parton densities with x) provided the structure functions are reliably measured up to $x \sim 0.8$.

The evolution equations allow one to calculate the parton densities $A^{i}(x,Q^2)$ provided they are given at some reference point Q_0^2. The densities $A^{i}(x,Q_0^2)$ are not predicted by perturbative QCD. They are usually parametrized based on plausible theoretical assumptions concerning their behaviour near the end points $x = 0$, 1, e.g.

$$
\begin{aligned}
xA^{NS}(x,Q_0^2) &= a_{NS}x^{\mu_{NS}}(1-x)^{\nu_{NS}}(1+\gamma_{NS}x), \\
xA^{SI}(x,Q_0^2) &= a_{SI}[x^{\mu_{SI}}(1-x)^{\nu_{SI}} + a_{SEA}x^{\mu_{SEA}}(1-x)^{\nu_{SEA}}], \\
xA^{G}(x,Q_0^2) &= a_G x^{\mu_G}(1-x)^{\nu_G}\,.
\end{aligned}
\qquad (30)
$$

At low Q_0^2, we expect from Regge theory and the quark counting rules: $\mu_{SI} \approx \mu_{NS} \geqslant 1-\alpha_\rho(0) \cong 0.5$, $\nu_{SI} \approx \nu_{NS} \approx 3$, $\mu_{SEA} \approx \mu_G \approx 0$, $\nu_G \geqslant \nu_{SI}+1$ and $\nu_{SEA} \geqslant \nu_G+1$. QCD evolution increases (decreases) the exponents ν_i (μ_i) with Q^2: $\nu_i \to \infty$, μ_{NS}, $\mu_{SI} \to 1-\alpha_\rho(0)$ and μ_{SEA}, $\mu_G \to \mu_\infty$, where $-1 < \mu_\infty < 0$. The high-x behaviour of the gluon distribution, compatible with QCD at sufficiently high Q_0^2, is, in fact, of the form [35]:

$$xA^G \propto (1-x)^{\nu_{SI}+1}/\ln\frac{1}{1-x} ,$$

which suggests a x-dependence of the exponent ν_G in eq. (30), e.g.

$$\nu_G(x) = \nu_{SI}+1+\ln(1+\nu_0\ln\frac{1}{1-x})/\ln\frac{1}{1-x} . \qquad (30')$$

In the limit $x \to 1$ the quantity ν_0 is related to ν_{SI} by [36]:

$$\nu_0 = [\gamma - \frac{3}{20} + \psi(2+\nu_{SI})]^{-1} ,$$

where γ and $\psi(z)$ are the Euler constant and ψ-function, respectively; $\nu_0 = 0.5$–0.4 at $\nu_{SI} = 3$–5. In the region of moderate or low x, however, the effective value of ν_0 may substantially differ from this estimate ($\nu_0 = 1$ is simply assumed in ref. [35]). Eq. (30') yields $\nu_G(x)$ decreasing with x from $\nu_{SI}+\nu_0+1$ to $\nu_{SI}+1$, the decrease being quite slow except for regions near the end points $x=0$ (at $\nu_0 \gg 1$) and $x=1$.

It is important to provide a sufficient flexibility of the parton x-parametrizations at $Q^2 = Q_0^2$ in order to not bias the comparison of the QCD predictions with data. In particular, number of parameters describing the quark densities should be comparable with the number of measured x-intervals. Concerning the gluon density, its contribution to the structure functions and to the scaling violations rapidly vanishes with x and becomes small at $x > 0.3$. Thus the simple parametrization in eq. (30), even with $\mu_G = 0$ (at not too high Q_0^2), appeares to be sufficient at present experimental errors.

The evolution equations (16) can be solved numerically using a suitable algorithm [37-39]. Although straitforward, this method is not cheap in terms of computer time and meets a problem of accumulation of the rounding errors when evolving at very large scales. Therefore a number of analytic methods has been developed to solve these equations with lower price.

The simplest and fastest possibility is to use plausible parametrizations for the parton x, Q^2-distributions and determine the parameters in such a way that the evolution equations are approximately satisfied. Thus in refs. [40-42] the parameters are determined by minimizing deviations of the first 10-20 Mellin moments of these distributions from the QCD predictions, while in refs. [35,43,44], the parameters responsible for the Q^2 dependence are calculated exactly in the limits $x \to 0, 1$. The achieved accuracy, several % ($\sim$0.5%) in former (latter) case in the kinematic region of interest, is satisfactory for many purposes but it may be insufficient when the most precise data are analyzed. A drawback may be also limited flexibility of the parametrizations.

Another method [16] exploits the inverse Mellin transform

$$f(x) = \frac{1}{2\pi i} \int_{-i\infty}^{+i\infty} dn\; x^{-n} f(n,Q^2) \ , \tag{31}$$

which is performed numerically in finite and carefully chosen bounds allowing one to achieve the required accuracy. A minor drawback is that analytical expressions for the moments of the parton densities must be provided.

The other methods are based on the expansion of a structure function or parton densities in a series of orthogonal polynomials. In principle, they allow one to solve the evolution equations with any reasonable accuracy.

Originally, Bernstein polynomials were used in ref. [45] to expand a structure function with the expansion coefficients expressed through its Mellin moments given by QCD eqs. (7') and (19). The convergence of this series appeares however quite slow. The method was further developed and applied in refs. [28,46] – the structure function was represented by a convolution of the parton densities $A^i(x,Q_0^2)$ with the integration kernels given in a form of fast converging serieses.

In refs. [47,48], Laguerre polynomials were used to expand the densities $A^i(x,Q^2)$. The evolution of their Laguerre moments is known in an analytical form. The densities at a reference point Q_0^2 are represented by their Laguerre moments which has an advantage (however minor) as compared with the usual apriori parametrizations of their x-dependence.

An important variation of the polynomial reconstruction method - Jacobi polynomial expansion - was proposed in ref. [49] and further studied, developed and applied to the analysis of experimental data in refs. [50-54,6,8,10]. It is discussed in some detail in the next Section.

3.2 Jacobi polynomial reconstruction of structure functions

Given the Jacobi moments $a_m(Q^2)$, a function $f(x,Q^2)$ may be reconstructed in a form of the series

$$xf(x,Q^2) = \lim_{M\to\infty} x^{\beta}(1-x)^{\alpha} \sum_{m=0}^{M} a_m(Q^2)\Theta_m^{\alpha\beta}(x), \tag{32}$$

where the Jacobi polynomials

$$\Theta_m^{\alpha\beta}(x) = \sum_{j=0}^{m} c_j^m(\alpha,\beta)x^j$$

satisfy the orthogonality relation with the weight $x^{\beta}(1-x)^{\alpha}$. The Jacobi moments are just linear combinations of the Mellin ones:

$$a_m(Q^2) = \sum_{j=0}^{m} c_j^m(\alpha,\beta)f(j+2,Q^2) \ . \tag{33}$$

Their Q^2-dependence thus simply follows from the QCD eqs. (7') and (19). It was shown that a fast convergence of the reconstruction series can be achieved when appropriately choosing the weight function to factor out an essential part of the structure function x-dependence. As a result, not only the first $N_{max} = M+1$ Jacobi or Mellin moments of the truncated series are exactly equal to the given (QCD) values (due to the orthogonality relation) but also higher moments approximately satisfy this equality [50] (the weight function causes a rapid vanishing of the Jacobi moments).

Originally, a Q^2-dependent weight function (with $\alpha = \alpha(Q^2)$) was proposed. Later on, it was recognized [50,52,53] that a good reconstruction accuracy (better than 1%) can be obtained with constant values of α and β, and, a reasonable number N_{max} of the terms retained in the series. As expected, the choice $\alpha \approx 3$ and β

≈ 0.5 for the weight function parameters appears to be optimal in the nonsinglet case. For a singlet structure function given in eq. (30) with $\mu_{SI} = 0.25$, $\nu_{SI} = 3$, $\mu_{SEA} = 0$ and $\nu_{SEA} = 8$, two sets of optimal α, β values have been found [53]: $\alpha \approx 3$, $\beta \approx 0.2$ and $\alpha \in (-0.8,\ 3.3)$, $\beta \approx -0.8$. The relation $\beta_1 \approx \beta_2+1$ between the two β-values is merely consequence of the polynomial expansion.

The accuracy analysis of ref. [53] does not take into account a rapid Q^2-evolution of the sea quarks and gluons. Since the evolution effectively leads to the appearance of a negative power of x in their x-distributions [35], we may expect decreasing the optimal β-value with Q^2. This is indeed confirmed (fig. 2) by the analysis of the r.m.s. relative reconstruction accuracy

$$\Delta_2^M(Q^2) = \left\{\frac{1}{N}\sum_{i=1}^{N}\left[\frac{F_2^M(x_i,Q^2)-F_2(x_i,Q^2)}{F_2(x_i,Q^2)}\right]^2\right\}^{1/2} \qquad (34)$$

of the BCDMS proton structure function ($N = 11$). The index M indicates that the structure function was reconstructed from the first $M+1$ moments. We have approximated the structure function by

$$F_2(x,Q^2) \cong \sum_{j=1}^{3} c_j x^{\beta_j}(1-x)^{\alpha_j}, \qquad (35)$$

where the parameters c_j, α_j, β_j, $j = 1, 2$ and 3, are calculated from the first three evolved NLO-moments of the NS, SI and gluon densities , respectively. The QCD mass-scale parameter Λ, as well as the parameters in eqs. (30) defining the initial densities at $Q^2 = 5\ GeV^2$, were determined by a QCD fit of the BCDMS proton structure function [8]. The approximation (35) is sufficient for studying the reconstruction accuracy, and, as the moments of its rhs are exactly known, it avoids the necessity of the "exact" solution of the evolution equations for this purpose.

It may be seen from figures 2 and 3 that an optimal choice of the weight function parameters α and β in the case of a proton structure function would be $\alpha \in (0,\ 4)$ and β close to -1 or $\beta \approx -0.15$. In the BCDMS kinematic range this choice garanties $\Delta_2^{11} <$ 0.3%. This is more than one order better result as compared with the case of the constant weight function (Legendre polynomial expansion). For the longitudinal structure function, due to a substantial gluon contribution, the reconstruction accuracy appears to be much worse: $\Delta_L \approx 50\ \Delta_2$ at the optimal values $\alpha \approx 6$ and β close to -1. Such an inaccuracy is still acceptable since it is comparable with the uncertienties due to the higher-order corrections, and, it is compensated by a small F_L-contribution to the cross section (up to several % in a few high-y BCDMS points). Figures 2 and 3 also indicate, in contrast with the nonsinglet case [52], the sensitivity of the reconstruction accuracy to the analyzed Q^2-interval. Clearly, this is a consequence of a fast singlet evolution in the low-x region.

The dependence of the reconstruction accuracy on the number N_{max} of the terms in the reconstruction series and on the length of the IBM computer word is displayed in fig. 4. It may be seen that the single precission is sufficient - up to $N_{max} = 8$, the double precission - up to $N_{max} = 22$, and, that the reconstruction accuracy blows up at $N_{max} = 44$ even if the maximal word length of REAL*16 has been used. It also follows from fig. 4 that the IBM double precission allows one to achieve the reconstruction accuracy by about one order better than in the case of the single one, while further doubling of the word length is less effective. We may conclude that the computer precission practically limits the number of the retained terms to $N_{max} < 20$. Due to rapidly increasing computer time with N_{max}, an optimum seems to be N_{max} = 10-15. In this case, as may be seen from fig. 4, there is only a minor difference in reconstruction accuracies corresponding to the exact and numerical calculations of the initial moments from eqs. (30).

It should be noted [32] that the convergence of the reconstruction series destroyes at $N_{max} > 10$ if the QCD moments have been calculated neglecting the corrections to the OPE next-to-leading anomalous dimensions arising from the substitutions (22).

We may conclude that a simple and a cheap tuning of the Jacobi polynomial reconstruction of both the transverse and the longitudinal structure functions is possible to make the reconstruction uncertienties in the predicted cross section less than a fraction of %, i.e. negligable even in the case of presently most precise BCDMS data.

3.3 *QCD fits*

The Jacobi moments $a_m(Q^2)$, unlike the Mellin ones, rapidly vanish with m and represent an independent, and, in the limit of precise data over the whole x-range, uncorrelated piece of information. It is therefore convenient to parametrize a nonsinglet structure function at a reference point Q_0^2 in terms of a few first Jacobi moments [50]; the required parametrization of the corresponding Mellin moments is merely given by the inverse of eq. (33). Of course, in the singlet case, two sets of the initial Jacobi moments should be given, corresponding to the quark singlet and the gluon part of the structure function. In principle, it is possible to consider the Mellin moments of the parton densities at Q_0^2 as free parameters [53]. This is however of a little practical use due to a large number of such parameters (increasing with N_{max}) and large correlations among them. The starting values of the Mellin moments can be also parametrized with the help of eqs. (30). This parametrization appears to be sufficiently flexible for the analysis of present data and is used in the following.

To perform the complete QCD fits, we have modified the computer code used in ref. [53] for a LO singlet analysis of the EMC iron data, and, in ref. [6], for a NLO, essentially nonsinglet, analysis of the BCDMS carbon data.

Thus the parameters in eqs. (30) are determined together with the QCD mass-scale parameter Λ by fitting the QCD predictions to the cross section data points. These points are sometimes given in a form of the function (see, e.g. [5,9,55]):

$$F_2^0(x,Q^2;E) = \frac{K[x,Q^2;E,R(x,Q^2)]}{K(x,Q^2;E,0)} F_2(x,Q^2), \tag{36}$$

which coincides with the structure function $F_2(x,Q^2)$ at $R(x,Q^2) = 0$. The K-function is the factor in square bracket in eq. (6).

Approximate procedures are often used assuming $R(x,Q^2) = 0$ or parametrizing it in a simple form (see, e.g., the critics raised in ref. [56]). We compare the cross section data with the complete next-to-leading order QCD prediction containing both the structure functions F_2 and F_L calculated in the $\overline{MS}$ renormalization scheme. Different weight functions are used to optimize the Jacobi reconstruction of these structure functions - the corresponding exponents α, β may be treated as free parameters of the fit. The procedures are also included into the code allowing one to take into account the preasymptotic corrections (flavour threshold-, target mass- and higher twist- ones) to the leading twist massless theory (see Sect. 4).

The new code has been already applied for QCD fits of the BCDMS hydrogen data [8,10]. The reference point was chosen at a value $Q_0^2 = 5\ GeV^2$ and the NLO mass-scale parameter Λ was defined by eq. (14''). An excellent agreement of the QCD predictions with the data is demonstrated in figs. 5 and Table 1. The results of

Table 1. The results of NLO leading-twist QCD fits to the BCDMS hydrogen data [9] ($\Lambda_{\overline{MS}}$ in MeV), assuming four massless flavours and parametrizing the parton densities according to eqs. (30) at a reference point $Q_0^2 = 5\ GeV^2$; $\mu_{SEA} = \mu_G = 0$, the momentum sum rule is used. The kinematic cuts of ref. [10] are applied; in particular, $x > 0.06\ (0.25)$ in a SI+NS (NS) fit.

Fit	μ_{NS}	ν_{NS}	γ_{NS}	a_{NS}	μ_{SI}	ν_{SI}	$\langle x_q \rangle$	ν_{SEA}	a_{SEA}	ν_G	$\Lambda_{\overline{MS}}$	$\frac{\chi^2}{DOF}$
SI+NS	0.5 ±0.2	3.5 ±0.2	10 ±2	1.1 ±0.2	0.8 ±0.1	4.5 ±0.6	0.45 ±0.08	13 ±4	0.17 ±0.05	9.5 ±1.5	205 ±21	$\frac{258}{270}$
NS	0.6 ±0.2	3.5 ±0.3	0.1 ±0.8	2.2 ±0.7	-	-	-	-	-	-	198 ±20	$\frac{178}{198}$

the fits well agree with the ones [10,11] obtained by a different method (based on a numerical solution of the evolution equations [39]), except for a slight systematic difference of 10-15 MeV in the NLO Λ-values. Almost half of this difference is due to ~30% underestimation of the R-function (see discussion at the end of Section 2.4) in latter fits. The two methods would be fully equivalent provided [52] the exact solution of the NLO equation (14) for $\alpha_s(Q^2)$ is used instead of the equally valid NLO approximation in eq. (14''); in the former method, also the exact solutions of the NLO Mellin transformed evolution equations should be used, e.g. the nonsinglet H-function in eq. (20) should be replaced by the one in eq. (20'). These equations may substantially differ if a reference point Q_0^2 has been chosen too low. It apppears, however, that the fits are not sensitive to this difference even at Q_0^2 as low as $5\ GeV^2$.

Since a "fine tuning" of the x-parametrizations was applied in the second method, a good agreement of the χ^2-values also indicates a sufficient flexibility of the quark parametrizations in eqs. (30). We have confirmed this with the help of polynomial modifications of these parametrizations and found that the subsequent change of Λ is negligable ($< 2\ MeV$).

Note that the large errors of the parameters of the quark densities arise due to substantial correlations among them. However, these parameters, being determined essentially by the x-dependence of the structure functions averaged over Q^2, are practically decorrelated from the QCD mass-scale parameter Λ, which measures the size of the scaling violations. This circumstance makes the deep-inelastic lepton scattering a good place for testing QCD (see Section 3.4).

A surprisingly soft gluon distribution has been obtained in the NLO. Thus, parametrizing the gluon density according to eq. (30) with $\mu_G = 0$, the fitted exponent $\nu_G \approx 10$ is about twice the one expected from the quark counting rule and found in the LO analysis. Note that the neglect of the longitudinal structure function ($R = 0$) would lead to still a softer gluon distribution (ν_G by 30–40% higher) and to Λ higher by 15 MeV. The gluon parametrization should be however considered only as an effective one in the range $0.06 \leqslant x \leqslant 0.30$, where an essentially nonzero gluon contribution is required by the measured scaling violations (compare full and dotted curves with dashed one in fig. 5d and see also fig. 4 of ref. [10]). Thus, at $\nu_G = 10\ (5)$ the gluon contribution to the scaling violation $\partial lnF_2/\partial lnQ^2$ becomes comparable with the experimental error at $x = 0.22\ (0.35)$. The

BCDMS data are thus not sufficiently precise to reliably determine the exponent ν_G responsible for the gluon distribution at $x > 0.3$. In fact, replacing ν_G by the ansatz (30') with $\nu_0 = 5$, corresponding to $\nu_G^{eff} \approx 9.5$ at $x < 0.3$ and $\nu_G^{eff} \to 5.5$ at $x \to 1$, we reproduce the results of Table 1. A reasonable fit can be also achieved with a smaller value of ν_0 provided the exponent μ_G is treated as free parameter. E.g. choosing $\nu_0 = 1$, i.e. $\nu_G^{eff} \approx 6.5$ at $x < 0.3$, and fitting $\mu_G = -0.16 \pm 0.07$, $\Lambda_{\overline{MS}} = 216 \pm 22$ MeV (other parameters practically coincide with the ones in Table 1), the χ^2 increases by ~1 unit only.

In the fits we have constrained the size of the gluon density with the help of the momentum sum rule (9). This may be questionable as it requires an interpolation of the singlet quark and gluon densities into the unmeasured region of $x < 0.06$. It appeares, however, when treating both $\langle x_q \rangle$ and $\langle x_G \rangle$ as free parameters and assuming $\mu_{SEA} = \mu_G = 0$, that the results of Table 1 remain practically unchanged (except for 50% increase of the error in ν_G), and, that the sum rule is well satisfied: $1 = 1.05 \pm 0.13$.

The softness of the gluon distribution makes it possible to neglect its contribution in the evolution equations at sufficiently large x-values and determine Λ with the help of a more constrained nonsinglet analysis. The results of NS fits shown in fig. 6 indicate that the BCDMS data are insensitive to the gluon distribution at $x \geqslant 0.25$. In this x-interval the NLO nonsinglet approximation, as compared with the complete SI+NS treatment, yields Λ by ~ 10 MeV lower (see Table 1 and ref. [10]). In the LO this shift is about three times as large due to harder gluon distribution. To estimate the influence of the gluon density on the distortion of Λ in a NS fit, we plot in fig. 7 the ν_G-dependence of $\Lambda_{\overline{MS}}$ fitted in the full x,Q^2-region ($x > 0.06$) and - in the NS one ($x > 0.25$). It may be seen that a negative correlation between these parameters weakens in latter case, as expected due to rapid vanishing with x of the gluon contribution in the scaling violations (fig. 5d). Since a fit in the full x,Q^2-region yields $\nu_G > 5$ at a level of two standard deviations (in agreement with the lower limit $\nu_{SI}+1$ following from the ansatz (30')), and, $\langle x_G \rangle = 0.44 \pm 0.06$ at $\nu_G = 5$, we may conclude from fig.

7 that a NS fit underestimates $\Lambda_{\overline{MS}}$ by $5\pm^{15}_{5}$ MeV at the same confidence level. We may also conclude that the uncertienty in $\Lambda_{\overline{MS}}$, introduced by the gluon distribution, is by ~60% larger in the full kinematic region than in the NS-one.

The N_{max}-dependence of the results of NLO fits is displayed in fig. 8. In agreement with the reconstruction accuracy analysis, the results of NS and SI+NS fits show stable behaviour for $N_{max} \geqslant 8$ and $N_{max} \geqslant 10$–13, respectively.

Since the parton x-distributions evolve with Q^2, a check of the Q_0^2-independence of the fitted Λ and χ^2 values also provides a flexibility test of the initial x-parametrizations in eqs. (30) in a given Q_0^2-region. The results of NS and complete SI+NS QCD fits shown in fig. 9 as functions of Q_0^2 indicate sufficient flexibility of the NS x-parametrization, and - some problem with the singlet quark and the gluon ones; the use of the latter with $\mu_{SEA} = \mu_G = 0$ slightly underestimates $\Lambda_{\overline{MS}}$ at $Q_0^2 > 50\ GeV^2$. This problem arises due to a fast Q^2-evolution in the low-x region and it may be cured by treating the exponents μ_{SEA} and μ_G as free parameters. Thus choosing, e.g. $Q_0^2 = 200\ GeV^2$ and fitting $\mu_{SEA} = \mu_G \approx -0.3$, $\nu_G \approx 11$, we recover $\Lambda_{\overline{MS}} \approx 200\ MeV$ obtained at low Q_0^2-values.

3.4 Testing QCD

Even the BCDMS data are not sufficiently precise for tests of the most specific QCD prediction - asymptotic freedom - manifested by vanishing of $\alpha_s(Q^2)$ (or the scaling violations $\propto \alpha_s$) with Q^2. The corresponding curvature of lnF_k in lnQ^2 is practically hidden in the statistical errors. Present data thus allow one to obtain only an average coupling $\langle\alpha_s\rangle$ in the measured Q^2-region. The fitted value of Λ then practically coincides with the one following from equation $\alpha_s(\langle Q^2\rangle) = \langle\alpha_s\rangle$.

In such a situation, the well-known illustrative representation of perturbative QCD predictions in terms of the logarithmic slopes $\partial lnF_2/\partial lnQ^2$ (see, e.g., [1]) approximately substitutes the global QCD description. It follows from the evolution equations, in particular, from the LO nonsinglet production, whereas the charged current top production may give a non-negligable effect depending on the top quark mass.

It appeares that the χ^2 of the fits to the BCDMS hydrogen data as well as the fitted gluon density are practically insensitive to the number of flavours used to calculate the evolution (the splitting functions). At the same time, the mass-scale parameter Λ is strongly correlated to this number: changing $f = 4$ to $f = 5$ decreases $\Lambda_{\overline{MS}}$ by $60\ MeV$. Assuming the bottom threshold at $Q^2 = (5\pm2)m_b^2$ we get for the shift of $\Lambda_{\overline{MS}}(f=4)$ due to the FTC a value of $-5\pm^{3}_{10}\ MeV$. The uncertienty in Λ due to parameter p in eq. (49) is less than $1\ MeV$. We may conclude that the influence of the FTC on the QCD tests and the determination of α_s is negligable at present.

4.3 Target mass- and higher twist- corrections (TMC and HTC)

In the simple model of free massless partons the TMC arise from the intrinsic transverse parton momentum [82-84,19]. Somewhat misleading name of these corrections is due to the fact that, as a consequence of kinematic constraints, they vanish as a square of the target mass M. Thus the contribution of the quark i to the structure functions F_2 and F_L is given by:

$$F_2^i(x,Q^2) = (\tfrac{x}{\xi})^2(1+\varepsilon)^{-3/2}[1+\frac{6\langle k_{i\perp}{}^2\rangle_0}{Q^2}]\ \tilde{F}_2^i(\xi),$$

$$F_L^i(x,Q^2) = (\tfrac{x}{\xi})^2(1+\varepsilon)^{-1/2}[\tilde{F}_L^i(\xi)+\frac{4\langle k_{i\perp}{}^2\rangle_0}{Q^2}\ \tilde{F}_2^i(\xi)]. \qquad (50)$$

Here $\langle k_{i\perp}{}^2\rangle_0$ is the mean transverse momentum squared of the i-th quark:

$$\langle k_{i\perp}{}^2\rangle_0 = M^2\frac{x\xi^2}{(1+\varepsilon)^{1/2}}\int_\xi^1 \frac{d\xi'}{\xi'^2}\ \tilde{F}_2^i(\xi')[1+2\frac{M^2}{Q^2}\ \frac{x(\xi'-\xi)}{(1+\varepsilon)^{1/2}}]/\tilde{F}_2^i(\xi) \qquad (51)$$

and ξ is the well-known Nachtmann variable:

$$\xi = 2x/[1+(1+\varepsilon)^{1/2}], \qquad (52)$$

equation

$$\frac{\partial lnF_2^{NS}(x,Q^2)}{\partial lnQ^2} = \frac{\alpha_s(Q^2)}{2\pi}\int_x^1 \frac{dy}{y}\,\frac{F_2^{NS}(y,Q^2)}{F_2^{NS}(x,Q^2)}\,P_+^{(0)}(\frac{x}{y}), \tag{16'}$$

that the logarithmic slopes are roughly constant and proportional to $\langle\alpha_s\rangle$. Their x-dependence in the NS case is uniquely predicted by perturbative QCD (provided the structure function is measured up to sufficiently high values of x), while their size determines the free parameter of the theory: $\langle\alpha_s\rangle$ or Λ. It is convenient [6] to calculate both the average theoretical and experimental slopes with the help of a straight line fit according to the equation

$$lnF_2(x,Q^2) = a + b\cdot ln\frac{Q^2}{\langle Q^2\rangle_x}. \tag{37}$$

Thus assigning to the predicted points of the BCDMS proton structure function $F_2(x,Q^2)$ the experimental errors (285 points after application of the selection criteria of ref [10]) and fitting them by formula (37) in each x-interval, the corresponding total χ^2 of 1.8 units appears to be negligable as compared with χ^2= 243 of a similar fit to the data. This circumstance allows one to neglect the higher derivatives $\partial^k lnF_2/\partial(lnQ^2)^k$ and identify, within the errors, the parameters a and b with $lnF_2(x,\langle Q^2\rangle_x)$ and $\langle\partial F_2/\partial lnQ^2\rangle \cong \partial F_2(x,Q^2)/\partial lnQ^2|_{Q^2=\langle Q^2\rangle_x}$, respectively. An excellent agreement of the theoretical and experimental x-dependences of these quantities is demonstrated in figs. 5b-d. The corresponding χ^2s, $\chi^2(a)$ = 1.5 and $\chi^2(b)$ = 8.9, agree with the respective numbers of degrees of freedom $NDF(a) = N_x - NP_x$ = 1 and $NDF(b) = N_x - NP_Q$ = 9, where N_x= 11 is the number of x-intervals, NP_x= 10 is the number of parameters in the initial structure function x-parametrization and NP_Q= 2 is the number of parameters responsible for the Q^2-evolution (Λ and ν_G; a_G is fixed by the momentum sum rule, and, $\mu_G = 0$). Note that $\chi^2(a)$ merely tests the flexibility of the initial x-parametrization, while $\chi^2(b)$, as stressed by BCDMS collaboration [6,8,10], yields practically the only specific test of perturbative QCD for deep-inelastic scattering within the accuracy of present experiments. In the nonsinglet approximation, the slope test depends on Λ as practically the sole free parameter whereas in a full SI+NS analysis there is additional freedom due to the gluon distribution (the other parameters, and, to some extent also the parameters in the gluon distribution, eat the degrees of freedom in $\chi^2(a)$).

Though the comparison of the slopes merely reflects the quality of a global fit, dealing with the essentially compressed information it may yield a more stringent QCD test [6,8,10]. Thus eventual slope discrepancies may lead to an unacceptably large $\chi^2(b)$, and, at the same time still give the global χ^2 of a reasonable confidence level due to a large *NDF*. The analysis [6] of the iron EMC data may serve as an example.

The problem of an optimal binning for the χ^2 test is quite general - the integration over the bins which are not sensitive to the eventual discrepancy may increase the test selectivity. Another possibility is to use a $\Delta\chi^2$ test based on χ^2-comparison of two hypotheses. This test is practically independent on the binning provided the bins sensitive to differences are fine enough. It can be shown that the difference $\Delta\chi^2$ of the χ^2s corresponding to a global QCD fit (${\chi_{QCD}}^2$) and to the linear representation (37) of the data in each x-interval (${\chi_L}^2$) is given by

$$\Delta\chi^2 \equiv {\chi_{QCD}}^2 - {\chi_L}^2 = \chi^2(a,b) - {\tilde{\chi}_L}^2. \tag{38}$$

Here ${\tilde{\chi}_L}^2$ is the χ^2 of the straight line representation of the QCD predictions with the assigned experimental errors (1.8 units in the case of the BCDMS hydrogen data) and

$$\chi^2(a,b) = \sum_{i=1}^{N_x} \vec{\Delta}_i \, \hat{E}_i^{-1} \, \vec{\Delta}_i^T = \chi^2(a) + \chi^2(b) + 2\sum_{i=1}^{N_x} (\hat{E}_i^{-1})_{ab} \Delta a_i \Delta b_i, \tag{39}$$

where $\vec{\Delta}_i = (\Delta a_i, \Delta b_i)$, and, $\hat{E}_i^{-1}$ is the inverse error matrix resulting from the linear fit in the i-th x-interval. The *NDF* of $\Delta\chi^2$ equals to the difference of the numbers of free parameters of the two hypotheses: $NDF = 2N_x - (NP_x + NP_Q)$, i.e. $NDF \approx N_x - NP_Q$ at $NP_x \approx N_x$. The generalization of the $\Delta\chi^2$-test for the case of data sensitive to the curvature of $\ln F_2$ in $\ln Q^2$ is straightforward. The replacement of the linear representation in eq. (37) by a parabolic one leads to $\Delta\chi^2$ with $NDF = 3N_x - (NP_x + NP_Q)$, i.e. $NDF = 2N_x - NP_Q$ at $NP_x \approx N_x$.

In figs. 10-12 we compare various χ^2s obtained in a NLO fit of the BCDMS hydrogen data as functions of Λ and the gluon parameters ν_G and $\langle x_G \rangle$. Note that χ_L^2 depends on these parameters through the longitudinal structure function (see eq. (6)). It may be seen that eq. (39) is well satisfied. Besides, $\chi^2(b)$ and $\Delta\chi^2$ are close to each other; they are practically parallel as functions of Λ but not as functions of the gluon parameters. This is in accordance with a weak dependence of $\chi^2(a)$ on Λ and with a noticeable one on ν_G and $\langle x_G \rangle$. We may conclude that the $\chi^2(b)$- and $\Delta\chi^2$-tests are of similar selectivity. The latter is somewhat preferable as it takes into account all the available information, though, it has minor drawback being less robust -- more sensitive to the initial parton x-parametrizations.

4. Preasymptotic corrections

4.1 Higher-order corrections (HOC)

The problem of HOC is closely related to the one of the renormalization scheme (RS) dependence of a truncated perturbation series (see, e.g., [18,20,22,54,57-64]). Thus the QCD predictions for a physical quantity ρ obtained to a finite order $O(\alpha_s^m)$:

$$\rho^{(m)} = \alpha_s^q \cdot (1 + r_1\alpha_s + .. + r_m\alpha_s^m)$$

differ in various schemes at $(m+1)$-th order when expanded in powers of the coupling constant in some reference RS. At m-th order, the RS is specified by m conditions. The corresponding unphysical parameters may be identified as the renormalization point μ and the beta function coefficients β_i, $i = 2,.. m$ [18]. Thus the RS-dependence of the NLO predictions is entirely equivalent to the problem of the best choice of the renormalization point within one particular scheme. Changing the renormalization point μ by another one $\tilde{\mu} = \mu/æ$, the NLO coefficients in the expansions (10) or (10') of the coefficient functions and the mass-scale parameter Λ become æ-dependent, e.g. [14,23]:

$$\tilde{B}^{NS(1)}_{2,n} = B^{NS(1)}_{2,n} - \gamma^{(0)}_{+}(n)\cdot ln æ,$$
$$\tilde{R}^{NS(2)}_{L,n} = R^{NS(2)}_{L,n} - [\gamma^{(0)}_{+}(n) + 2\beta_0]\cdot ln æ,$$
$$\tilde{\Lambda} = æ\cdot\Lambda. \tag{40}$$

It is implied $\Lambda/\mu \ll æ \ll \mu/\Lambda$ so that the æ-rescaling of the parameter Λ in eq. (40) is approximately equivalent to the rescaling of α_s:

$$\tilde{\alpha}_s = \alpha_s\cdot(1 + \frac{\alpha_s}{4\pi}\beta_0 ln æ^2). \tag{40'}$$

Choosing the $\overline{MS}$ scheme as the reference RS and assuming $f = 4$, we have, e.g. $æ = 2.17$ for the MOM scheme [60], or, $æ = 0.377$ for the MS scheme [14]. The complete NLO contribution to the predicted scaling violations, e.g. to

$$\rho_{2,n} = - \frac{8\pi}{\gamma^{(0)}_{+}(n)} \frac{\partial ln f^{NS}_2(n,Q^2)}{\partial ln Q^2} =$$
$$= \tilde{\alpha}_s\cdot[1 + \frac{\tilde{\alpha}_s}{4\pi} \frac{\gamma^{(1)}_{+}(n)+2\beta_0\tilde{B}^{NS(1)}_{2,n}}{\gamma^{(0)}_{+}(n)} + \ldots], \tag{41}$$

or, to

$$\rho_{L,n} = - \frac{8\pi}{\gamma^{(0)}_{+}(n)+2\beta_0} \frac{\partial ln f^{NS}_L(n,Q^2)}{\partial ln Q^2} =$$
$$= \tilde{\alpha}_s\cdot[1 + \frac{\tilde{\alpha}_s}{4\pi} \frac{\gamma^{(1)}_{+}(n)+2\beta_1+2\beta_0\tilde{R}^{NS(2)}_{L,n}}{\gamma^{(0)}_{+}(n)+2\beta_0} + \ldots], \tag{41'}$$

is, of course, independent of the RS, as would be full all order calculation. However, since we truncate the calculation in the NLO, different choices for æ yield different estimates of the higher-order terms. This is demonstrated in fig. 13 where we plot $\rho^{(1)}_{2,n}(æ)$ and the ratio $\rho^{(1)}_{2,n}(æ)/\rho^{(1)}_{2,n}(1)$ at $\Lambda = 200$ MeV, $\mu = Q = 10$ GeV as functions of æ and $n = 2, 6, 10$. Similar curves, with the renormalization point μ by another one $\tilde{\mu} = \mu/\ae$, the NLO coefficients in the expansions (10) or (10') of the coefficient functions and the mass-scale parameter Λ become $\ae$-dependent, e.g. [14,23]:

$$\tilde{B}^{NS(1)}_{2,n} = B^{NS(1)}_{2,n} - \gamma^{(0)}_{+}(n)\cdot ln\ae,$$
$$\tilde{R}^{NS(2)}_{L,n} = R^{NS(2)}_{L,n} - [\gamma^{(0)}_{+}(n) + 2\beta_0]\cdot ln\ae,$$
$$\tilde{\Lambda} = \ae\cdot\Lambda. \tag{40}$$

It is implied $\Lambda/\mu \ll \ae \ll \mu/\Lambda$ so that the $\ae$-rescaling of the parameter Λ in eq. (40) is approximately equivalent to the rescaling of α_s:

$$\tilde{\alpha}_s = \alpha_s\cdot(1 + \frac{\alpha_s}{4\pi}\,\beta_0 ln\ae^2). \tag{40'}$$

Choosing the $\overline{MS}$ scheme as the reference RS and assuming $f = 4$, we have, e.g. $\ae = 2.17$ for the MOM scheme [60], or, $\ae = 0.377$ for the MS scheme [14]. The complete NLO contribution to the predicted scaling violations, e.g. to

$$\rho_{2,n} = -\frac{8\pi}{\gamma^{(0)}_{+}(n)}\,\frac{\partial ln f^{NS}_2(n,Q^2)}{\partial ln Q^2} =$$
$$= \tilde{\alpha}_s\cdot[1 + \frac{\tilde{\alpha}_s}{4\pi}\,\frac{\gamma^{(1)}_{+}(n)+2\beta_0\tilde{B}^{NS(1)}_{2,n}}{\gamma^{(0)}_{+}(n)} + \,..\,], \tag{41}$$

or, to

$$\rho_{L,n} = -\frac{8\pi}{\gamma^{(0)}_{+}(n)+2\beta_0}\,\frac{\partial ln f^{NS}_L(n,Q^2)}{\partial ln Q^2} =$$
$$= \tilde{\alpha}_s\cdot[1 + \frac{\tilde{\alpha}_s}{4\pi}\,\frac{\gamma^{(1)}_{+}(n)+2\beta_1+2\beta_0\tilde{R}^{NS(2)}_{L,n}}{\gamma^{(0)}_{+}(n)+2\beta_0} + \,..\,], \tag{41'}$$

is, of course, independent of the RS, as would be full all order calculation. However, since we truncate the calculation in the NLO, different choices for $\ae$ yield different estimates of the higher-order terms. This is demonstrated in fig. 13 where we plot $\rho^{(1)}_{2,n}(\ae)$ and the ratio $\rho^{(1)}_{2,n}(\ae)/\rho^{(1)}_{2,n}(1)$ at $\Lambda = 200$ MeV, $\mu = Q = 10$ GeV as functions of $\ae$ and $n = 2, 6, 10$. Similar curves, with the axima shifted by $\Delta æ \approx 1.9$, are obtained for the quantity $\rho_{L,n}$. ote that a weak n-dependence of $\rho^{(1)}_{2,n}(æ)$ (especially for $6 \leqslant n$ 10, corresponding roughly to the x-interval of NS fits) explains he same χ^2s of the BCDMS LO and NLO fits [6,8,10] – the NLO $_{2,n}$-values may be well approximated by the LO one: $\rho^{(0)}_{2,n} = \alpha_s(LO)$ $1.3\alpha_s(\overline{MS})$; this leads to $\Lambda_{LO} \approx \Lambda_{\overline{MS}}$ in the BCDMS Q^2-range.

Though the RS dependence problem can be solved only by alculating still the higher-order terms in the expansion series the results at high orders may be, however, of a little value due o asymptotic character of the perturbation series), a number of uggestions how to choose the optimal RS in a finite-order alculation (minimizing the HOC) have been discussed. For example, t was suggested to fix the RS by the requirement of fastest pparent convergence (FAC), i.e. by the one of vanishing orrection to the LO result [61,62] (see also similar scheme nvariant approaches of refs. [59,63,64,20,54]), or, by the rinciple of minimal sensitivity (PMS) of the result on the nphysical parameters characterizing the RS [18]. It follows from hese studies that there is no universal optimal RS. Thus the FAC r PMS schemes depend on the particular structure function and on he number n of its moment. For the structure function F_2 the atter dependence is indicated by the arrows on the curves in fig. 3. The corresponding $æ_n$-values in the case of longitudinal tructure function are higher by ~ 1.9 (PMS) and ~ 1.6 (FAC).

Fortunately, within the accuracy of present data the igher-order uncertienty (RS-dependence) of the predicted -dependence of the scaling violations is rather small. In articular, fig. 14 indicates only a weak æ-dependence of the χ^2 f a NS fit to the BCDMS hydrogen data within the range of pproximate validity of the NLO expansion (in which the -rescalings in eqs. (40) and (40') yield near-by results – closed nd open circles). Clearly this is a consequence of similar -dependences of the scaling violations at various x or n, i.e. – f a weak n-dependence of the ratio $\rho_{2,n}(æ)/\rho_{2,n}(1)$ (fig. 13), llowing one to compensate the change of æ merely by a shift of α_s. At the same time, this explains substantial dependence of the itted value of $\Lambda_{\overline{MS}}$ on æ displayed in fig. 14.

The n-dependence of the æ-values characterizing the optimal schemes could, in principle, essentially modify the one of the scaling violations. However, since these schemes extrapolate (with the help of optimization criteria) our knowledge of the NLO corrections to the higher-order ones, and, since the former introduce minor change in the n-dependence of the scaling violations in a wide æ-range, this modification appears to be minor as well. Thus the n-dependences of the scaling violations in the FAC and PMS optimal schemes are close to the one in the MOM scheme (fig. 13).

It follows that the check of perturbative QCD with the help of measured scaling violations and the determination of the mass-scale parameter Λ are quite different tasks - the uncertienty due to higher orders being probably small in former but not in latter case. Based on fig. 14, we may estimate that a NLO fit at æ $= 1$ yields $\Lambda_{\overline{MS}}$ with an uncertienty of $\pm^{120}_{30}$ MeV (i.e. four times as large as the difference between NLO eqs. (14') and (14'')). Such an uncertienty is also indicated by recent calculation [65] of the third-order correction to $R_{e^+e^-}$ in the $\overline{\text{MS}}$ scheme. This correction leads to $\sim$ 10% decrease of α_s at $\sqrt{s}= 34$ GeV, and, according to eq. (15) for $\alpha_s^{(2)}$, - to $\sim$ 40% decrease of $\Lambda_{\overline{MS}}$.

However, as compared with $R_{e^+e^-}$, there is an additional problem due to the higher-order contributions containing terms proportional to the powers of $\alpha_s ln(1-y)$ and $\alpha_s lny$ $(x \leqslant y \leqslant 1)$ which destroy the validity of the perturbative QCD predictions for the inclusive leptoproduction at high and low values of x. Various procedures for resummation of these terms have been suggested. Concerning the low-x region, the perturbative QCD predictions appear to be valid until x as small as 10^{-3}-10^{-4} [66,67]. The situation in the high-x region is less clear since the effect of the resummation (exponentiation) is almost as important as the ambiguity associated with it [68]. Fortunately, in the BCDMS kinematic range, the resummation of the terms containing powers of $ln(1-y)$ (or ln^2n) leads only to a few MeV change of the NLO Λ-value. E.g., using eq. (20') for the NS H-function, and, exponentiating analogically the coefficient function [26]:

$$C_k^{NS}(n,Q^2) = [1 + \frac{\beta_1}{\beta_0}\frac{\alpha_s(Q^2)}{4\pi}]^{\frac{\beta_0}{\beta_1}} B_\pm^{NS}(n) \quad ,$$

a NLO fit of BCDMS hydrogen data yields, in the nonsinglet approximation, Λ by 5 MeV higher and χ^2 by 1 unit better than the standard fit.

Related to the high-x problem there is a question of the HOC starting at three loops. Thus a consideration of the evolution in terms of the timelike variable $W^2 = m^2 + Q^2(1-y)/y$ (the effective mass-squared of a final state in the photon-parton subprocess) instead of $q^2 = -Q^2$ leads to the effective replacement in eqs. (14)-(15) [69]:

$$\ln\frac{Q^2}{\Lambda^2} \rightarrow (\ln^2\frac{Q^2}{\Lambda^2} + \pi^2)^{1/2} \quad ,$$

indicating that the contribution of the $O(\alpha_s^{\ 3})$ terms may be substantial. Neglecting other possible HOC, it would mean less steep running of $\alpha_s(Q^2)$ as compared with the prediction of eq. (14), i.e. the NLO Λ-value increasing with Q^2. Thus to the BCDMS NLO value Λ = *210 MeV* would correspond *230 (240) MeV* at UNK (HERA) and *300 MeV* at asymptotic energies. This effect should be trackable in the experiments planned to measure running of α_s at SPS CERN and UNK with the statistical error of a few MeV in Λ [70].

We may conclude that at present the HOC-uncertienties in the predicted x-dependence of the scaling violations seem to be practically negligable as compared with the experimental errors. At the same time the HOC may lead to an uncertienty as large as ~ 10% in α_s (or in $F_L \propto \alpha_s$) and ~ 40% in Λ. The clarification of the HOC would be clearly of great importance for the comparison of measured Λ with lattice calculations and for the derivation of any prediction from Grand Unified Theories (e.g. of the proton lifetime $\propto \Lambda^4$).

4.2 Flavour threshold corrections (FTC)

The corrections due to flavour excitation treshold are of the order $O(m_i^2/Q^2)$ at Q^2 much larger than a heavy quark mass squared m_i^2. They become large at $Q^2 < m_i^2$, since, according to the intuitive decupling theorem [71], the contribution of a heavy flavour vanishes at $Q^2 \ll m_i^2$. Generally, the FTC arise from the mass dependence of $\alpha_s(Q^2)$, coefficient functions and splitting functions (anomalous dimensions). There was some hope [72-74] that the FTC can be calculated within the MOM renormalization scheme. In this scheme, the mass-dependence of α_s and the gluon-gluon splitting function is merely connected with the replacement of the number of flavours by an effective one:

$$f \to \tilde{f} = \sum_{i=1}^{f} K(m_i^2/Q^2) \approx \sum_{i=1}^{f} 1/(1 + 5m_i^2/Q^2) \equiv \sum_{i=1}^{f} \Delta\tilde{f}_i \ . \qquad (42)$$

Thus in the LO, beta function renormalization group equation (11), neglecting a weak Q^2-dependence of the quark masses, yields the running coupling constant in the form (13), with the number of flavours f in eq. (12) for β_0 replaced by

$$\tilde{f}' = \sum_{i=1}^{f} \Delta\tilde{f}'_i \approx \sum_{i=1}^{f} \ln[(Q^2 + m_i^2)/(\Lambda^2 + m_i^2)]/\ln(Q^2/\Lambda^2). \qquad (43)$$

The new effective number of flavours in eq. (43) saturates quite slowly as compared with $\tilde{f}(Q^2)$. Thus, using $m_c = 1.5\ GeV/c^2$, $m_b = 4.5\ GeV/c^2$ and $\Lambda = 200\ MeV$, we have at $Q^2 = 100\ GeV^2$: $\Delta\tilde{f}'_c = 0.29$, $\Delta\tilde{f}'_b = 0.09$ as compared with $\Delta\tilde{f}_c = 0.90$, $\Delta\tilde{f}_b = 0.50$. It may be seen from fig. 15 that the usual ansatz of four massless flavours with appropriately rescaled Λ-value provides reasonable approximation to the mass-dependent $\alpha_s(Q^2)$. Even better approximation is achieved when calculating $\alpha_s(Q^2)$ with the number of massless flavours appropriate for a given Q^2-range and requiring the continuity of $\alpha_s(Q^2)$ at flavour excitation thresholds. The corresponding mass-scale parameters Λ_f are only weakly dependent on the threshold positions [75]. Choosing them at $(1-5)m_i^2$, we have in the NLO: $\Lambda_3:\Lambda_4:\Lambda_5 \approx 1.3:1:0.65$. Since the mean approximation accuracy is much better than the accuracy of present measurements of $<\alpha_s>$ (~2.5% in the case of BCDMS hydrogen data), we may conclude that the mass-dependence of $\alpha_s(Q^2)$ is of minor practical importance.

The situation with the mass-dependence of the coefficient and splitting functions is not so simple: the results of refs. [72,73] appear to be renormalization prescription- and gauge- dependent. Of course, the ambiguities cancell when the mass-dependence of the coefficient functions is taken into account [76]. Unfortunately, they cancell together with all the mass-dependence besides the "trivial" one in α_s and the gluon-gluon anomalous dimension.

Therefore, similar to refs. [77-79], we estimate the FTC with the help of a phenomenological approach based on the perturbative QCD calculation of the γ-gluon fusion process $\gamma g \to \bar{q}_i q_i$. The contribution of this process to the structure function $f_k(x,Q^2)$ is given by [80]:

$$f_k^{iG}(x,Q^2) = \int_x^1 \frac{dy}{y} \frac{\alpha_s(m_i^2)}{2\pi} e_i^2 \cdot h_k^i(\frac{x}{y},Q^2)\cdot G(y,m_i^2), \qquad (44)$$

where, e.g.

$$h_L^i(z,Q^2) = 2z(1-z)\{2v-(1-v^2)ln[(1+v)/(1-v)]\}\theta(x_0-z),$$
$$v = (1-4m_i^2/W^2)^{1/2}, \quad x_0 = 1/(1+4m_i^2/Q^2). \qquad (45)$$

Here, v is the heavy-quark velocity in the $\bar{q}_i q_i$ rest frame and $W^2 = Q^2(1/z-1)$ is the invariant mass squared of the heavy-quark system. The corresponding result of the renormalization group approach, expanded in $ln(Q^2/Q_0^2)$ at $Q^2 \approx Q_0^2 \approx m_i^2$, reads as follows:

$$f_k^{iG}(n,Q^2) = \frac{\alpha_s(m_i^2)}{2\pi} e_i^2 \cdot \frac{1}{2J}\{B_{k,n}^{G(1)} - C_k^q(n,Q^2)\int_{Q_0}^{Q} \frac{d\mu}{\mu}\gamma_n^{iG(0)}\}G(n,Q_0^2). (46)$$

Comparing eqs. (44) and (46) we could try to extract the mass-dependence of the coefficient functions and - of the gluon-quark anomalous dimension. Evidently, there is no unique way to do this. Thus in ref. [78] all the mass-dependence of the transverse function h_2 was incorporated into the modified gluon-heavy quark splitting function, while the one of the longitudinal function h_L - into the modified gluon coefficient function. In ref. [77], both the quark and the gluon coefficient functions were modified. To retain the simplicity of the $\overline{MS}$ renormalization scheme, we follow ref. [77] (see also [81]) and treat the mass-dependence of the anomalous dimensions in a simplified way assuming them mass-independent, i.e. the Q^2-evolution mass-independent, in a Q^2-range between the neighbouring heavy flavour excitation thresholds Q_i^2 (eq. (42) indicates $Q_i^2 \approx 5m_i^2$), and, include the explicite mass-dependence entirely into the coefficient functions. The standard QCD formula is then replaced, in the NLO, by

$$
\begin{aligned}
f_k(n,Q^2) &= C_k^q(n,Q^2)\cdot[A^{NS}(n,Q^2)+A^{SI}(n,Q^2)] + \sum_{i=1}^{f} e_i^2 \tilde{C}_k^{iG}(n,Q^2)G(n,Q^2) + \\
&+ e_c^2[\tilde{C}_k^c(n,Q^2)-C_k^q(n,Q^2)]\cdot[c(n,Q^2)+\bar{c}(n,Q^2)] + \\
&+ e_b^2[\tilde{C}_k^b(n,Q^2)-C_k^q(n,Q^2)]\cdot[b(n,Q^2)+\bar{b}(n,Q^2)] + \dots\,. \qquad (47)
\end{aligned}
$$

The modified coefficient functions $\tilde{C}_k$ are normalized in such a way that, at $Q^2 \gg m^2$,

$$
\tilde{C}_k^i = C_k^q\,, \quad \tilde{C}_k^{iG} = \frac{1}{f}\, C_k^G\,,
$$

where $C_k^q = C_k^{NS} = C_k^{SI}$ in the NLO. The mass-dependence of the modified coefficient functions in the $\overline{MS}$ scheme has not yet been calculated. Unfortunately, it cannot be determined from eqs. (44)-(46) unambiguously. Thus using the relation

$$
\ln\frac{1+v}{1-v} = \ln(Q^2/m_i^2) + \ln[(1+v)^2(1-z)/4z],
$$

we may, like in ref. [77], absorb the mass-dependence of the coefficient in front of the diverging term $\ln(Q^2/m_i^2)$ in eq. (44) into the modified quark coefficient function $\tilde{C}_k^i$, the remaining one - into the modified gluon coefficient function:

$$
\begin{aligned}
\tilde{C}_L^{iG(1)}(z,Q^2) &= 2z(1-z)\{2v-(1-v^2)\ln[(1+v)^2(1-z)/4z]\}, \\
\tilde{C}_2^{iG(1)}(z,Q^2) &= v[-1+8z(1-z)-z(1-z)4m_i^2/Q^2] + \\
&+ [1-2z(1-z)+4z(1-3z)m_i^2/Q^2-8z^2m_i^4/Q^4]\ln[(1+v)^2(1-z)/4z]\}. \qquad (48)
\end{aligned}
$$

n the case of the longitudinal structure function, we might not are about the logarithmic divergence at $Q^2 \gg m_t^2$, which is uppressed by the factor $(1-v^2)$, and, like in ref. [78], put $\tilde{C}_L^{t(0)}$ 0 and absorb all the mass-dependence into the modified gluon oefficient function. More generally, we can modify both the oefficient functions in eqs. (48), e.g. by the replacement:

$$ln[(1+v)^2(1-z)/4z] \rightarrow ln\frac{1+v}{1-v} - v^p ln(Q^2/m_t^2), \qquad (49)$$

$\geqslant 0$, and, define the heavy quark coefficient functions in a orresponding way. The latter are actually not needed, since, in iew of the approximations used, we may neglect the small last erms in eq. (47) related to the heavy-quark distributions; these erms vanish in the limits of large and small Q^2s as compared with m_t^2. To estimate the FTC uncertienty we plot in fig. 16 the atio $r^{(1)} = F_L^{cG(1)}/F_L^{uG(1)}$ of the yields of the c- and u-quarks in he longitudinal photon-gluon fusion calculated with $p = 0$ (i.e. sing eq. (48)) and $p = 4$ (close to the case of no subtraction in ubstitution (49), i.e. close to the ansatz of ref. [78]). A aster saturation of the heavy quark contribution to F_L at smaller is seen. There is an additional uncertienty connected with the ass-dependence of the α_s^2-contribution to F_L. We simply assume $C_{L,n}^{G(2)}$, or, $R^G(x)$ to be mass-independent. Near the threshold it eads to a much slower saturation of the α_s^2-contribution of a eavy quark to F_L than of the α_s-one: $r^{(2)} \approx x_0^5 \cdot r^{(1)}$. In spite of onsiderable uncertienties of the FTC, their influence on the tructure functions is rather small. First, the gluon contribution F_k^G is moderate even at x as small as 0.1 (a few % to F_2 and $\sim 60\%$ o F_L) and rapidly decreases with x (fig. 17). Second, even if we ompare the cases of no ($m_t = 0$) and the total ($m_t^2 \gg Q^2$) uppression, the change of the gluon contribution is not very arge (less than 40% for F_L^G); for F_L it corresponds to the maximal ossible uncertienty of $\sim 12\%$ at $x = 0.1$, and, - to a much smaller ne at higher x-values (fig. 16).

A noticeable manifestation of the FTC can be expected at HERA here the region of very small x will be covered. The calculations f ref. [79] indicate negligable FTC due to charm and bottom production, whereas the charged current top production may give a non-negligable effect depending on the top quark mass.

It appeares that the χ^2 of the fits to the BCDMS hydrogen data as well as the fitted gluon density are practically insensitive to the number of flavours used to calculate the evolution (the splitting functions). At the same time, the mass-scale parameter Λ is strongly correlated to this number: changing $f = 4$ to $f = 5$ decreases $\Lambda_{\overline{MS}}$ by $60\ MeV$. Assuming the bottom threshold at $Q^2 = (5\pm2)m_b^2$ we get for the shift of $\Lambda_{\overline{MS}}(f=4)$ due to the FTC a value of $-5\pm^{3}_{10}\ MeV$. The uncertienty in Λ due to parameter p in eq. (49) is less than $1\ MeV$. We may conclude that the influence of the FTC on the QCD tests and the determination of α_s is negligable at present.

4.3 *Target mass- and higher twist- corrections (TMC and HTC)*

In the simple model of free massless partons the TMC arise from the intrinsic transverse parton momentum [82-84,19]. Somewhat misleading name of these corrections is due to the fact that, as a consequence of kinematic constraints, they vanish as a square of the target mass M. Thus the contribution of the quark i to the structure functions F_2 and F_L is given by:

$$F_2^i(x,Q^2) = (\frac{x}{\xi})^2(1+\varepsilon)^{-3/2}[1-\frac{6\langle k_{i\perp}{}^2\rangle_0}{Q^2}]\ \tilde{F}_2^i(\xi),$$

$$F_L^i(x,Q^2) = (\frac{x}{\xi})^2(1+\varepsilon)^{-1/2}[\tilde{F}_L^i(\xi)+\frac{4\langle k_{i\perp}{}^2\rangle_0}{Q^2}\ \tilde{F}_2^i(\xi)]. \tag{50}$$

Here $\langle k_{i\perp}{}^2\rangle_0$ is the mean transverse momentum squared of the i-th quark:

$$\langle k_{i\perp}{}^2\rangle_0 = M^2\frac{x\xi^2}{(1+\varepsilon)^{1/2}}\int_\xi^1 \frac{d\xi'}{\xi'^2}\ \tilde{F}_2^i(\xi')[1+2\frac{M^2}{Q^2}\ \frac{x(\xi'-\xi)}{(1+\varepsilon)^{1/2}}]/\tilde{F}_2^i(\xi) \tag{51}$$

and ξ is the well-known Nachtmann variable:

$$\xi = 2x/[1+(1+\varepsilon)^{1/2}], \tag{52}$$

ere ε is defined in eq. (4). The function $\tilde{F}_2^i(\xi)$ is related to e Lorentz invariant quark wave function squared $f(\xi')$:

$$\tilde{F}_2^i(\xi) = \frac{\pi}{2} M^2\xi^2 \int_{\xi}^{1} d\xi' f(\xi'), \quad \xi' = 2k\cdot p/M^2;$$

and p are the quark and target 4-momenta, respectively. In boratory frame the lower and upper integration limits correspond $k_\perp = 0$ and $k_0 = m/2$. Note that the kinematic constraint $k_0^{lab} \leqslant$ /2 implies:

$$k_\perp^2 \leqslant \frac{M^2}{4}[M^2+ Q^2 \frac{1-x}{x}]/[M^2+ \frac{Q^2}{4x^2}] \rightarrow M^2x(1-x) \leqslant M^2/4, \qquad (53)$$

ere the arrow indicate a limit $Q^2 \gg M^2$. In this limit $F_2^i(x,Q^2) \rightarrow$ (ξ), so that the function $\tilde{F}_2^i$ can be identified as the asymptotic ructure function F_2^i. Note that $\tilde{F}_L^i(\xi) = 0$ in the considered odel. Adding the contributions from the light quarks, and, eglecting the ones from the heavy quarks, we get the usual form the TMC as given in eqs. (50) with $F_k^i \rightarrow F_k$, $\tilde{F}_k^i \rightarrow \tilde{F}_k$ and $\langle k_{i\perp}{}^2\rangle_0$ $\langle k_\perp{}^2\rangle_0$. Switching on the interaction ($\alpha_s \neq 0$), it seems easonable to assume that eqs. (50) remain valid but with the unctions $\tilde{F}_k(\xi)$ replaced by the corresponding QCD structure unctions $\tilde{F}_k(\xi,Q^2)$, logarithmically depending on Q^2.

Using the BCDMS hydrogen data as an input, we have found that e mean transverse momentum squared of the quarks in a proton eighted by $e_i{}^2$) is practically independent on Q^2 and can be arametrized as:

$$\langle k_\perp{}^2\rangle_0 = 0.95\ M^2x^2(1-x)/(1+3.35x)\ . \qquad (54)$$

his parametrization has correct limiting behaviour at $x \rightarrow 0,\ 1$ d its accuracy is better than 5% at x = 0.05-0.8, Q^2 = 10-200 eV^2. At moderate x-values it yields $\langle k_\perp{}^2\rangle_0 \approx 0.04\ GeV^2$ as xpected from uncertienty relation for a typical hadron size of ~ 1 m. Using further the high-x approximation $F_2(x,Q^2) \propto (1-x)^\nu$, ere $\nu \approx 3.5$ in the Q^2 range of 10-$10^2\ GeV^2$, we can represent s. (50) in the order $O(M^2/Q^2)$ with a reasonable accuracy as follows:

$$F_2(x,Q^2) \cong \{1 + \frac{6\langle k_\perp{}^2\rangle_0}{Q^2} + \frac{M^2}{Q^2}[\frac{\nu x^3}{1-x} - 4x^2]\}\cdot\tilde{F}_2(x,Q^2),$$

$$F_L(x,Q^2) \cong [1 + \frac{M^2}{Q^2}\,\frac{(\nu+1)x^3}{1-x}]\cdot\tilde{F}_L(x,Q^2)+\frac{4\langle k_\perp{}^2\rangle_0}{Q^2}\,\tilde{F}_2(x,Q^2). \quad (50')$$

It may be seen from fig 18 that the TMC to $F_2(x,Q^2)$ is practically negligable at $x < 0.55$ ($<1\%\cdot 10\ GeV^2/Q^2$ at $Q^2 > 10\ GeV^2$), but rapidly increases at higher values of x. The TMC to $F_L(x,Q^2)$ is relatively very large at moderate values of x and Q^2. E.g. $\sim 100\%$ correction arises at $x = 0.55$, $Q^2 = 10\ GeV^2$ mainly from the second term in eq. (50) and becomes even larger at $x \to 1$ due to the first one. At lower x, where F_L essentially deviates from zero, the TMC is much less important. This is demonstrated in fig. 19 where we plot the proton function $R(x,Q^2)$, defined in eq. (5), and the ratio of the R-functions with TMC and/or HTC neglected in the nominator one.

There are however problems in the above approach. First, eqs. (50) yield nonvanishing structure functions for unphysical values of $1 < x \leqslant 1/(1-M^2/Q^2)$. This effect presumably arises from the mismatch between the spectrum of states in perturbative QCD (quarks and gluons) and the observed spectrum of physical particles, and, cannot be cured by switching on the interaction with the spectator quarks through a truncated series of the HTC [85,86]. Fortunately, this overestimation vanishes as $(M^2/Q^2)^\nu$, and, in fact, can be avoided in a finite order expansion of the TMC in inverse powers of Q^2, (see, e.g. eqs. (50')). Second, the restriction of $k_\perp{}^2$ in eq. (53), following from the free parton approximation, is in apparent contradiction with the uncertienty principle in the boundary regions $x \to 0$, 1, or, - in the case of a small target mass. To solve this problem, the simple picture of on-shell partons with intrinsic transverse momentum should be improved and generalized in the presence of interaction. It is well-known that both the kinematic and dynamical power corrections are controled by the transverse components of momenta and the gluon field. The complete QCD result can be formally written in the form of eqs. (50) corrected by the contribution of higher twist terms calculated in the limit of zero target mass:

$$HTC = TMC + HTC_0 .$$

Thus, for the twist-4 corrections HTC_0 to eqs. (50), we have [85]:

$$\Delta F_2(x,Q^2) = \frac{\Lambda^2}{Q^2}\, x\, [4T_1(x) - x\int dx_2 dx_1 \frac{\delta(x-x_2)-\delta(x-x_1)}{x_2-x_1}\, T_2(x_2,x_1)],$$

$$\Delta F_L(x,Q^2) = 4\,\frac{\Lambda^2}{Q^2}\, x\, T_1(x), \tag{55}$$

where $T_1(x)$ and $T_2(x_2,x_1)$ are certain parton correlation functions which measure the transverse momentum generated by the interaction together with the transverse componets of the gluon field. They satisfy the relation

$$4\int dx T_1(x) = \int dx_2 dx_1 T_2(x_2,x_1) \tag{56}$$

and the positivity constraint

$$\Lambda^2 T_1(x)/\tilde{F}_2(x) + \langle k_\perp{}^2\rangle_0 > 0 . \tag{57}$$

At sufficiently high x-values the integration over the gluon momenta implicit in the definition of the correlation functions is dominated by the soft gluon region. Assuming the soft gluon approximation valid also at lower x-values, the x-dependence of T_1 and T_2 is essentially given by the shape of the quark distribution function $\tilde{F}_2(x)/x$, i.e. [87]:

$$\Lambda^2 T_1(x) \cong k^2\, \tilde{F}_2(x)/x ,$$

$$\Lambda^2 T_2(x_2,x_1) \cong k^2 \delta(x_2-x_1)\, \tilde{F}_2(x)/x . \tag{58}$$

For the twist-4 contributions in eqs. (55) we then have (see also [42]):

$$\Delta F_2(x,Q^2) = 4\,\frac{k^2}{Q^2}\, x\frac{\partial}{\partial x}\, \tilde{F}_2(x,Q^2),$$

$$\Delta F_L(x,Q^2) = 4\,\frac{k^2}{Q^2}\, \check{F}_2(x,Q^2) . \tag{59}$$

Besides, the positivity constraint (57) for the mean transverse parton momentum squared takes the form:

$$k^2 + \langle k_\perp{}^2 \rangle_0 > 0 \ . \qquad (57')$$

We may thus interpret the positive parameter k^2 as the mean transverse momentum squared generated dynamically. Its positivity follows from the constraint (57') taken at the boundary x-values where $\langle k_\perp{}^2 \rangle_0$ vanishes. From the twist-4 corrections to the Gross-Llewellyn Smith sum rule calculated in ref. [88] within three different approaches (the QCD sum rules, the vector dominance approximation and the nonrelativistic quark model) we may estimate $k^2 = 0.013\text{-}0.033\ GeV^2$. This is in agreement with the expectation of $k^2 \sim 1\ fm^{-2} = 0.04\ GeV^2$ following from the uncertienty relation.

The twist-4 corrections in eqs. (55), (59) contain only the two-fermion contributions. The four-fermion ones vanish for the longitudinal structure function but not for $F_2(x,Q^2)$. Their x-dependence is expected [89] to be similar to the one in eq. (59). Based on the bag model calculations in ref. [90] we may estimate the corresponding k^2 as $\sim 0.004\ GeV^2$.

The results of NS fits to the BCDMS hydrogen data, taking into account the HTC according to eqs. (50), (59), are given in Table 2 (Fit 1-3). The values of the parameter k^2 fitted in various kinematic regions agree within the errors with the theoretical expectation of $0.02\text{-}0.04\ GeV^2$. They should be compared with previous determinations of this parameter: $k^2 = 0.10 \pm 0.16\ GeV^2$ [91], $0.12\text{-}0.20\ GeV^2$ [86] and $0.04\text{-}0.12\ GeV^2$ [92], based on EMC-, EMC+neutrino- and SLAC-data, respectively. A systematic decrease of the fitted k^2-value when cutting low-y or low-Q^2 points may indicate the sensitivity of the fits to systematic uncertienties of the BCDMS data which are largest just in the low-y region.

Large $\Lambda_{\overline{MS}}$ errors in these fits result from a compatition of the scaling violations in $F_2(x,Q^2)$ predicted by the leading twist QCD evolution and the HTC in eq. (59), which have similar x-dependences in the moderate-x region. This leads to a flat χ^2 curve as a function of k^2 and to a substantial correlation between

Table 2. The results of NLO nonsinglet QCD fits to the BCDMS hydrogen data [9] as described in caption of Table 1 but taking into account the HTC according to eqs. (50), (59).

Fit	Q^2-cut GeV^2	y-cuts [10]	HTC_o eq.	$\Lambda_{\overline{MS}}$ MeV	k^2 $(GeV/c)^2$	χ^2/DOF
1	20	yes	(59)	204 ± 53	0.02 ± 0.03	174/197
2	10	yes		218 ± 46	0.04 ± 0.03	201/228
3	10	no		247 ± 36	0.06 ± 0.02	222/250
4	20	yes	(60)	$238 \pm ^{130}_{100}$	–	171/192
5	10	yes		$273 \pm ^{80}_{70}$	–	192/223
6	10	no		297 ± 70	–	212/245

Λ and k^2, as it is demonstrated in fig. 20. The correlation weakens with stronger low-Q^2 cut but it remains essential even at rather large Q^2. E.g. the correlation slope at $Q^2 > 10\ GeV^2$ decreases only by 30% at $Q^2 > 40\ GeV^2$.

The error in Λ becomes still larger if we do not fix the x-dependence of the HTC in F_2 according to eq. (59) and replace it by the ansatz:

$$\Delta F_2(x_i, Q^2) = \frac{a_i}{Q^2} F_2(x_i, Q^2), \tag{60}$$

where a_i is a free parameter in each x-interval (see Fit 4-6 in Table 2). The fitted values of the parameters a_i (Fit 5) are compared in fig. 18 with the prediction $4k^2x\frac{\partial}{\partial x}F_2(x,Q^2)$ of eq. (59). It may be seen that this prediction does not contradict with the BCDMS data, and, that the global power corrections are slightly negative in the moderate-x region whereas at large x they are dominated by the positive TMC. The small negative power corrections at moderate x qualitatively agree with the results of neutrino experiments [93]. However, they are in disagreement with rather large positive HTC required to tail the low-Q^2 SLAC data to the deep-inelastic muon-proton scattering data of EMC and BCDMS [3,55]. This discrepancy may be due to the twist-6 contribution $\propto 1/Q^4$ to the charged lepton deep-inelastic scattering, being dominant in the SLAC kinematic region but getting negligable in the CERN one. Note that the twist-6 contribution to neutrino scattering is expected to be negligable [88,94].

The negative power corrections in F_2 lead to a systematic decrease of the mass-scale parameter Λ with decreasing the lower Q^2-cut when fitting the scaling violations according to the leading-twist perturbative QCD prediction only. Such a correlation is demonstrated for the BCDMS hydrogen data in fig. 21 (partly it may be related to systematic uncertienties in the low-y region). For Q^2-interval of 20-$260\ GeV^2$ it becomes negligable as compared with experimental errors which justifies the use of the leading-twist approximation and allows one to perform a stringent test of perturbative QCD (see Section 3.4). A stringent QCD test is also possible in a Q^2-interval extended to lower values of Q^2 provided the x-dependence of the HTC is fixed acording to eqs. (50) and (59). At the same time the HTC may substantially modify the Λ-value fitted in the leading twist approximation even at $Q^2 >$ 20-$30\ GeV^2$. Thus taking $k^2 = 0.04\pm0.04\ GeV^2$ as a combined result of Table 2 (including systematic errors) we may conclude from fig. 20 that the standard NS fit of the BCDMS hydrogen data (Table 1) underestimates $\Lambda_{\overline{MS}}$ by $35^{+60}_{-50}\ MeV$.

5. Conclusions

The influence of various approximations and theoretical uncertienties on the determination of the QCD mass-scale parameter $\Lambda_{\overline{MS}}$ in a nonsinglet NLO fit (using eq. (14'') for $\alpha_s(Q^2)$ and assuming four massless flavours) to the BCDMS hydrogen data in the region: $x = 0.25$-0.8, $Q^2 = 20$-$260\ GeV^2$ (y-cuts of ref. [10] are applied) is summarized in Table 3.

The contribution of higher twists in the BCDMS proton structure function $F_2(x,Q^2)$ is found small and negative in the moderate-x region and $Q^2 > 10\ GeV^2$, and, in agreement with theoretical models, it is well described in terms of one parameter $k^2 = 0.02$-$0.04\ GeV^2$ - the transverse momentum squared generated dynamically. This circumstance allows one to use the BCDMS data

Table 3. Corrections and uncertienties for the parameter $\Lambda_{\overline{MS}}$ fitted in a leading-twist NS approximation from the BCDMS hydrogen data as described in caption of Table 1.

Source	$\Delta\Lambda_{\overline{MS}}$ MeV
NS approximation (gluon x-parametrization)	$5 \pm ^{15}_{5}$
Calculation and fit procedures	± 2
Quark x-parametrizations	± 2
HOC	$\pm ^{120}_{30}$
FTC	$-5 \pm ^{3}_{10}$
HTC eqs. (50), (59)	$35 \pm ^{60}_{50}$
eqs. (50), (60)	$42 \pm ^{130}_{100}$

for a stringent QCD test and a reliable determination of the mass-scale parameter Λ.

Combining the results of Tables 1-3 and ref. [10], we get:

$$\Lambda_{\overline{MS}} = 204 \pm 53(stat.) \pm 60(syst.) \pm ^{120}_{30}(theor.)\ MeV,$$

or, including the uncertienty due to the HTC into the theoretical error:

$$\Lambda_{\overline{MS}} = 230 \pm 20(stat.) \pm 60(syst.) \pm ^{140}_{60}(theor.)\ MeV.$$

The statistical error in former case is dominated by the effect of the HTC. It would be twice as large if the theoretical ansatz in eq. (59) is replaced by the phenomenological one in eq. (60). The theoretical error is dominated by the higher-order uncertienty.

The next generation experiments may decrease the statistical and systematical errors in $\Lambda_{\overline{MS}}$ at least 5 times [70] and thus make it possible to perform fine QCD tests: clarify running of α_s and the influence of the higher-order corrections. These measurements could be also of great importance for Grand Unified Theories provided the theoretical uncertienty in Λ will be diminished by the next-to-next-to-leading order calculations.

L. Lednicky

References

1. F.E.Close, "An Introduction to Quarks and Gluons", Academic Press, 1979.
2. T.Sloan, Proceedings of the Int. Europhysics Conf. on High Energy Physics, Uppsala, 1987.
3. R.Voss, Proceedings of the 1987 Int. Symp. on Lepton and Photon Interactions at High Energies, Hamburg, 1987; CERN/EP 87-223.
4. R.Mount, Proceedings of the XXIVth Int. Conf. on High Energy Physics, Munich, August 1988.
5. BCDMS, A.C.Benvenuti et al., Phys. Lett. 195B (1987) 91.
6. BCDMS, A.C.Benvenuti et al., Phys. Lett. 195B (1987) 97.
7. M.Virchaux, These, Universite Paris VII, 1988.
8. BCDMS, A.C.Benvenuti et al., JINR-E1-87-689, Dubna 1987.
9. BCDMS, A.C.Benvenuti et al., Phys. Lett. 223B (1989) 485.
10. BCDMS, A.C.Benvenuti et al., Phys. Lett. 223B (1989) 490.
11. A.Ouraou, These, Universite Paris XI, 1988.
12. A.D.Martin, W.J.Stirling, R.G.Roberts, RAL-88-023, Chilton 1988.
13. A.A.Akhundov et al., Sov. J. Nucl. Phys. 26 (1977) 660; 44(1986) 988; JINR E2-86-104, Dubna 1986;
    D.Yu.Bardin, N.M.Shumeiko, Sov. J. Nucl. Phys. 29 (1979) 499.
14. W.A.Bardeen et al., Phys. Rev. D19 (1978) 3998.
15. G.Altarelli, R.K.Ellis, G.Martinelli, Nucl. Phys. B157 (1979) 461;
    J.Kubar-Andre, F.E.Paige, Phys. Rev. D19 (1979) 221.
16. M.Diemoz et al., Z. Phys. C39 (1988) 21.
17. O.Tarasov, A.Vladimirov, A.Zharkov, Phys. Lett. 93B (1980) 429
18. P.M.Stevenson, Phys. Rev. D23 (1981) 2916; D27 (1983) 1968.
19. A.Buras et al., Nucl. Phys. B131 (1977) 308.
20. S.J.Maximov, V.I.Vovk, Phys. Lett. B199 (1987) 443; Yad. Fiz. 46 (1987) 961.
21. G.Altarelli, Phys. Rep. 81 (1982) 1.
22. D.W.Duke, R.G.Roberts, Phys. Rep. 120 (1985) 275.
23. A.Devoto et al., Phys. Rev. D30 (1984) 541;
    D.W.Duke, J.D.Kimel, A.D.Sowell, Phys. Rev. D25 (1982) 71.

24. J.L.Miramontes, J.Sanchez Guillen, E.Zas, Phys. Rev. D35 (1987) 863.
25. A.Buras, Rev. Mod. Phys. 52 (1980) 199.
26. G.Curci, W.Furmanski, R.Petronzio, Nucl. Phys. B175 (1980) 27.
27. E.G.Floratos, D.A.Ross, C.T.Sachrajda, Nucl. Phys. B129 (1977) 66; B139 (1978) 545 B152 (1979) 493.
28. A.Gonzalez-Arroyo, C.Lopez, F.J.Yndurain, Nucl. Phys. B153 (1979) 161;
A.Gonzalez-Arroyo, C.Lopez, Nucl. Phys. B166 (1980) 429.
29. E.G.Floratos, C.Kounnas, R.Lacaze, Nucl. Phys. B192 (1981) 417
30. I.Antoniadis, E.G.Floratos, Nucl. Phys. B191 (1981) 217.
31. D.A.Ross, C.T.Sachrajda, Nucl. Phys. B149 (1979) 497.
32. R.Lednicky, CERN/EP/NA4 Note 88-01.
33. D.I.Kazakov, A.V.Kotikov, Nucl. Phys. B307 (1988) 721.
34. M.J.Herrero, J.L.Miràmontes, Phys. Rev. D34 (1986) 138.
35. C.Lopez, F.J.Yndurain, Nucl. Phys. B171 (1980) 231; B183 (1981) 157.
36. A.V.Kotikov, JINR E2-88-422, Dubna 1988.
37. L.F.Abbott, R.M.Barnett, Ann. of Phys. 125 (1980) 276.
38. A.Devoto et al., Phys. Rev. D27 (1983) 508.
39. M.Virchaux, A.Ouraou, DPhPE 89-07, Saclay 1989.
40. A.Buras, K.J.F.Gaemers, Nucl. Phys. B132 (1978) 249.
41. I.S.Zlatev et al., Yad. Fiz. 35 (1982) 454;
V.A.Bednyakov et al., Yad. Fiz. 36 (1982) 745.
42. Yu.P.Ivanov, P.S.Isaev, Yad. Fiz. 38 (1983) 744.
43. B.Escoubes et al., Nucl. Phys. B242 (1984) 329.
44. A.V.Kotikov, S.J.Maximov, V.I.Vovk, ITP-89-64E, Kiev 1989.
45. F.J.Yndurain, Phys. Lett. 74B (1978) 68.
46. EMC, J.J.Aubert et al., Phys. Lett. B114 (1982) 291.
47. W.Furmanski, R.Petronzio, Nucl. Phys. B195 (1982) 237.
48. CHARM, F.Bergsma et al., Phys. Lett. 123B (1983) 269.
49. G.Parisi, N.Sourlas, Nucl. Phys. B151 (1979) 421.
50. I.S.Barker, C.B.Langensiepen, G.Shaw, Nucl. Phys. B186 (1981) 61.
51. I.S.Barker, B.R.Martin, G.Shaw, Z. Phys. C19 (1983) 147;
I.S.Barker, B.R.Martin, Z. Phys. C24 (1984) 255.

52. J.Chyla, J.Ramea, Z. Phys. C31 (1986) 151.
53. V.G.Krivokhizhin et al., Z. Phys. C36 (1987) 51. ✓
54. V.I.Vovk, Yad. Fiz. 50 (1989) 204.
55. EMC, J.J.Aubert et al., Nucl. Phys. B259 (1985) 189.
56. S.I.Bilenkaya, D.B.Stamenov, JINR E2-87-287, Dubna 1987.
57. F.J.Yndurain, Quantum Chromodynamics (Springer, Berlin, 1983)
58. A.N.Schellekens, Lett. Nuovo Cim. 24 (1979) 513.
59. A.A.Vladimirov, Yad. Fiz. 31 (1980) 1083.
60. W.Celmaster, R.J.Gonsalves, Phys. Rev. Lett. 42 (1979) 1435; Phys. Rev. D21 (1980) 3112.
61. G.Grunberg, Phys. Lett. 95B (1980) 70.
62. A.L.Kataev, N.V.Krasnikov, A.A.Pivovarov, Nucl. Phys. B198 (1982) 508.
63. A.Dhar, Phys. Lett. B128 (1983) 407;
A.Dhar, V.Gupta, Phys. Rev. D29 (1984) 2822.
64. D.I.Kazakov, D.V.Shirkov, Yad. Fiz. 42 (1985) 768.
65. S.G.Gorishny, A.L.Kataev, S.A.Larin, Phys. Lett. B212 (1988) 238.
66. L.V.Gribov, E.M.Levin, M.G.Ryskin, Phys. Rep. C100 (1983) 1.
67. J.Kwiecinski, Z. Phys. C29 (1985) 147; 561.
68. J.Chyla, J.Phys. G: Nucl. Phys. 12 (1986) 1297.
69. M.R.Pennington, G.G.Ross, R.G.Roberts, Phys. Lett. 120B (1983) 204.
70. C.Guyot et al.: "A new fixed-target experiment for precise tests of QCD", Proposal, Saclay, 14 March 1989.
71. T.Applequist, J.Carrazone, Phys. Rev. D11 (1975) 2856.
72. A.DeRujula, H.Georgi, Phys. Rev. D13 (1976) 1296;
H.Georgi, H.D.Politzer, Phys. Rev. D14 (1976) 1829.
73. B.J.Edwards, T.D.Gottschalk, Nucl. Phys. B196 (1982) 328.
74. Yu.P.Ivanov, Yad. Fiz. 44 (1986) 492.
75. W.Marciano, Phys. Rev. D29 (1984) 580.
76. S.Wada, Phys. Lett. 29B (1980) 163.
77. S.P.Luttrell, S.Wada, Nucl. Phys. B182 (1981) 381.
78. M.Gluck, E.Hoffmann, E.Reya, Z. Phys. C13 (1982) 119.
79. M.Gluck, R.M.Godbole, E.Reya, DO-TH 87/12, Dortmund, 1987.
80. E.Witten, Nucl. Phys. B104 (1976) 445.
81. J.C.Collins, Wu-Ki Tung, Nucl. Phys. B278 (1986) 934.

82. R.Barbieri et al., Nucl. Phys. B117 (1976) 50.
83. A.DeRujula et al., Ann. Phys. 103 (1977) 315.
84. M.Gluck, E.Reya, Nucl. Phys. B145 (1978) 24.
85. R.K.Ellis, W.Furmanski, R.Petronzio, Nucl. Phys. B212 (1983) 29.
86. J.L.Miramontes, J.Sanchez Guillen, Z. Phys. C41 (1988) 247.
87. R.K.Ellis, W.Furmanski, R.Petronzio, Nucl. Phys. B207 (1982) 1
88. V.M.Braun, A.V.Kolesnichenko, Nucl. Phys. B283 (1987) 723.
89. S.P.Luttrell, S.Wada, B.R.Webber, Nucl. Phys. B188 (1981) 219.
90. R.L.Jaffe, M.Soldate, Phys. Lett. 105B (1981) 467.
91. V.A.Bednyakov et al., Yad. Fiz. 40 (1984) 770.
92. J.L.Miramontes, M.A.Miramontes, J.Sanchez Guillen, US/FT-3/89, Santiago de Compostela 1989.
93. BEBC-WA59, K.Varvell et al., Z. Phys. C36 (1987) 1.
94. E.V.Shuryak, A.I.Vainshtein, Nucl. Phys. B199 (1982) 451; B201 (1982) 144.

Figure Captions

Fig. 1. The NLO- and the ratio of the LO- and NLO-predictions of perturbative QCD for the proton longitudinal structure function calculated with the help of BCDMS hydrogen data [9] neglecting flavour threshold-, target mass- and higher twist-corrections; $Q^2 = 10$ and $100\ GeV^2$.

Fig. 2. The relative reconstruction accuracy (34) vs the weight function exponent β; $\alpha = 3$, $N_{max} = 12$ and $Q^2 = 10$ and $200\ GeV^2$.

Fig. 3. The relative reconstruction accuracy (34) vs the weight function exponent α; $\beta + 1 = 10^{-5}$, $N_{max} = 12$ and $Q^2 = 10$ and $200\ GeV^2$.

Fig. 4. The relative reconstruction accuracy (34) vs the number $N_{max} = M + 1$ of the retained terms at various lengths of the IBM computer word: REAL*4 (dashed curve), REAL*8 (dashed-dotted curve) and REAL*16 (full curve); $\alpha = 3$, $\beta + 1 = 10^{-5}$ and $Q^2 = 25\ GeV^2$. The dotted curve corresponds to REAL*8 and a numerical integration of the x-parametrizations in eqs. (30).

Fig. 5. Comparison of the BCDMS proton structure function $F_2(x,Q^2)$ [8] with the result of a complete SI+NS QCD fit (full curves) described in caption of Table 1; dotted and dashed curves correspond to $\nu_G = 5$ and $\langle x_G\rangle = 0$, respectively. The quantities $F_2(x,\langle Q^2\rangle_x) = a(x)$ and $\langle\partial lnF_2/\partial lnQ^2\rangle = b(x)$ are determined by assigning to the experimental and theoretical points the statistical experimental errors and fitting them in each x-interval according to eq. (37).

Fig. 6. The low-x cut dependence of the results of NS leading-twist NLO fits to the BCDMS hydrogen data [9]; $Q^2 > 20\ GeV^2$, the y-cuts of ref. [10] are not applied.

Fig. 7. The ν_G-dependence of $\Lambda_{\overline{MS}}$ and $\Delta\chi^2 = \chi^2 - \chi^2(\nu_G{=}10)$ obtained in complete SI+NS QCD fits (described in caption of Table 1) to the BCDMS hydrogen data [9] in the full x,Q^2-region (closed circles) and in the NS-one (open circles); $\langle x_G\rangle = 0.5$. The upper and lower dotted curves represent $\Lambda_{\overline{MS}}$ fitted in the NS-region at $\langle x_G\rangle = 0.6$ and 0.4, respectively; the corresponding $\Delta\chi^2$s coincide within 0.3 units with the ones obtained at $\langle x_G\rangle = 0.5$. The dashed line represents the result of a NS fit.

Fig. 8. The N_{max}-dependence of the results of NS (open circles) and complete SI+NS (closed circles) NLO QCD fits (described in caption of Table 1) to the BCDMS hydrogen data [8]; $\Delta\chi^2 = \chi^2 - \chi^2(N_{max}=13)$. Typical statistical errors are shown at $N_{max} = 13$.
Fig. 9. The $Q_0{}^2$-dependence of the results of the same fits as described in caption of fig. 8; $\Delta\chi^2 = \chi^2 - \chi^2(Q_0{}^2 = 5\ GeV^2)$, $N_{max} = 11$.
Fig. 10. The $\Lambda_{\overline{MS}}$-dependence of the results of complete SI+NS NLO QCD fits to the BCDMS hydrogen data [8], as described in caption of Table 1 but without imposing the momentum sum rule (9); $N_{max} = 12$. The $\Delta\chi^2$ (dashed curve) and the χ^2s (full curves) are defined in eqs. (38), (39).
Fig. 11. The ν_G-dependence of the results of the same fits as described in caption of fig. 10.
Fig. 12. The $\langle x_G\rangle$-dependence of the results of the same fits as described in caption of fig. 10.
Fig. 13. The quantity $\rho^{(1)}_{2,n}(æ)$ and the ratio $\rho^{(1)}_{2,n}(æ)/\rho^{(1)}_{2,n}(1)$ as functions of the parameter æ specifying the renormalization scheme; $n = 2, 6, 10$. The quantity $\rho_{2,n}$ measures the scaling violations in a NS structure function F_2. It is calculated in the NLO according to eq. (41) with $\Lambda = 200\ MeV$ and $\mu = Q = 10\ GeV$. Various schemes are indicated by the arrows.
Fig. 14. The results of nonsinglet NLO QCD fits (described in caption of Table 1) to the BCDMS hydrogen data [9] as functions of the parameter æ specifying the renormalization scheme. Various schemes are indicated by the arrows.
Fig. 15. The LO mass-dependent running coupling constant $\alpha_s(Q^2)$ at $\Lambda = 200\ MeV$ (full curve) and its approximation $\alpha_s'(Q^2)$ calculated with four massless flavours and normalized to $\alpha_s(Q^2)$ at $Q^2 = 60\ GeV^2$ (dashed curve); see eqs. (12), (13), (43). The ratio α_s'/α_s is also shown (dashed curve). The dotted curve corresponds to $\alpha_s'(Q^2)$ calculated with the number of massless flavours f appropriate for a given Q^2-interval; the flavour excitation thresholds are chosen at $4m_i{}^2$ which implies $\Lambda_3 = 222\ MeV$, $\Lambda_4 = 180\ MeV$, $\Lambda_5 = 128\ MeV$.
Fig. 16. The dashed regions represent ratios of $\bar{c}c$ and $\bar{u}u$ production rates in the longitudinal photon-gluon fusion, and,

ratios of the NLO longitudinal proton structure functions calculated with $m_c = 1.5\ GeV/c^2$ and $m_c = 0$ (neglecting target mass- and higher twist-corrections). The upper and lower bounds correspond to $p = 0$ and 4, respectively (eqs. (48), (49)). Dashed curves represent ratios of the structure functions calculated with three (m_c=∞) and four massless flavours. $Q^2 = 10$ and $100\ GeV^2$.

Fig. 17. Relative gluon contribution to the proton longitudinal structure function calculated with $m_c = 1.5\ GeV/c^2$, $p = 4$ (neglecting target mass- and higher twist-corrections) at $Q^2 = 10\ GeV^2$ (full curve) and $100\ GeV^2$ (dashed curve).

Fig. 18. Power corrections to the proton structure function $F_2(x,Q^2)$ at $Q^2 = 60\ GeV^2$. The TMC (full curve) is calculated according to eq. (50). The HTC_0 result from NS-fits to the BCDMS hydrogen data [9] using eq. (59) ($k^2 = 0.04\ GeV^2$ - dashed curve) and eq. (60) (points) in the region $x > 0.25$, $Q^2 > 10\ GeV^2$; y-cuts of ref. [10] are applied.

Fig. 19. The structure function $R = \sigma_L/\sigma_T$ at $Q^2 = 10$ and $100\ GeV^2$, obtained in a complete NLO QCD fit (described in caption of Table 1) to the BCDMS hydrogen data [9]. The flavour threshold corrections are taken into account according to eqs. (47)-(49), the target mass- and higher twist-ones - according to eqs. (50) and (59) with $k^2 = 0.04\ GeV^2$. Spreading of the curves corresponds to the dashed regions in fig. 16. Ratios of the R-functions are also shown with neglected HTC_0 (dashed curves) and HTC_0+TMC (full curves) in the nominator one.

Fig. 20. Results of NS fits to the BCDMS hydrogen data as functions of the transverse momentum squared k^2 generated dynamically (see eq. (59)); $\Delta\chi^2 = \chi^2 - \chi^2(k^2=0)$. Closed circles, open circles and crosses correspond to Fit 1,2 and 3 in Table 2. Dotted line indicates $\Lambda_{\overline{MS}}$ fitted with $HTC = 0$.

Fig. 21. The low-Q^2 cut dependence of the results of NS leading-twist NLO fits to the BCDMS hydrogen data [9]; $x > 0.25$, the y-cuts of ref. [10] are not applied.

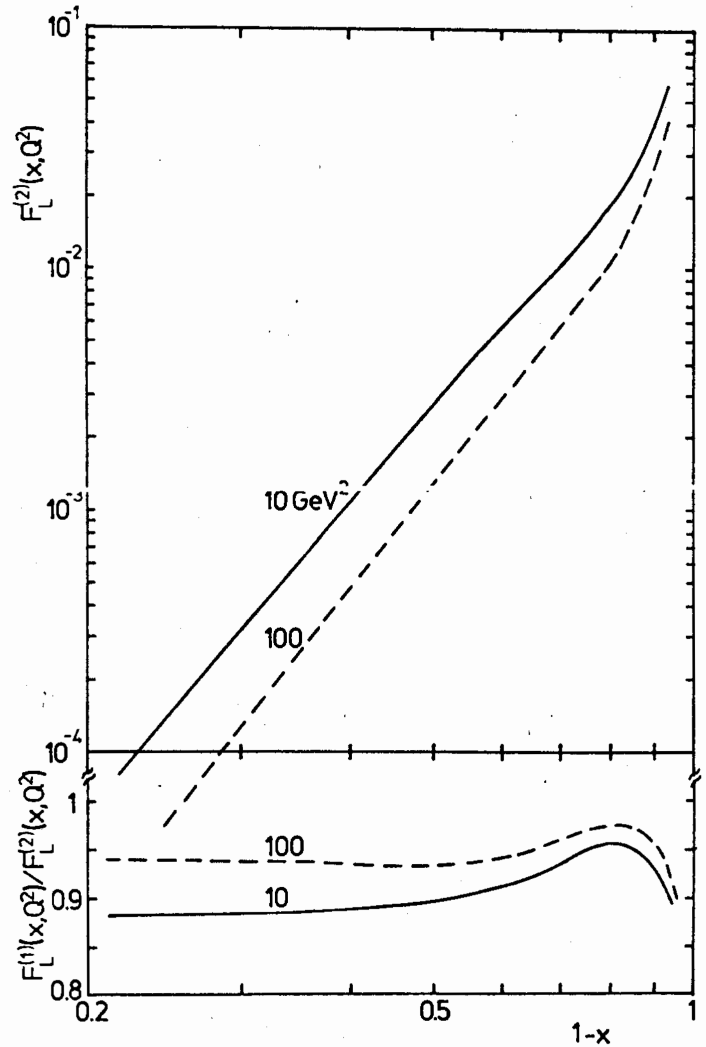

10^{-1}
$F_L^{(2)}(x,Q^2)$
10^{-2}
10^{-3}
10 GeV^2
100
10^{-4}
$F_L^{(1)}(x,Q^2)/F_L^{(2)}(x,Q^2)$
1
100
0.9
10
0.8
0.2
0.5
1
1-x

Fig. 1

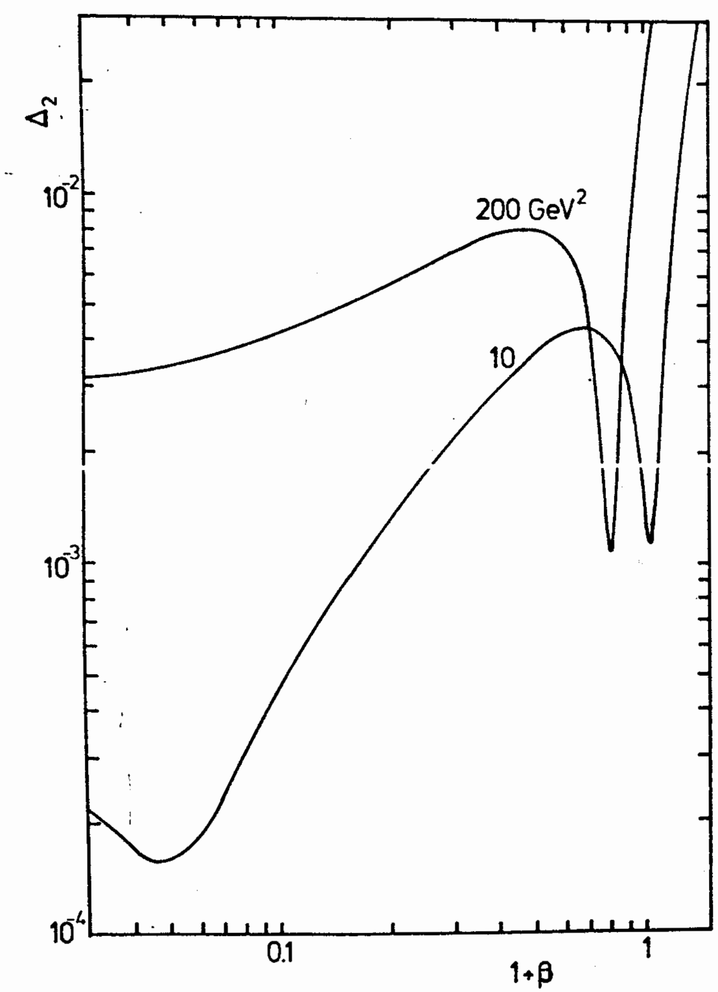

Δ_2
10^{-2}
200 GeV^2
10
10^{-3}
10^{-4}
0.1
1
1+β

Fig. 2

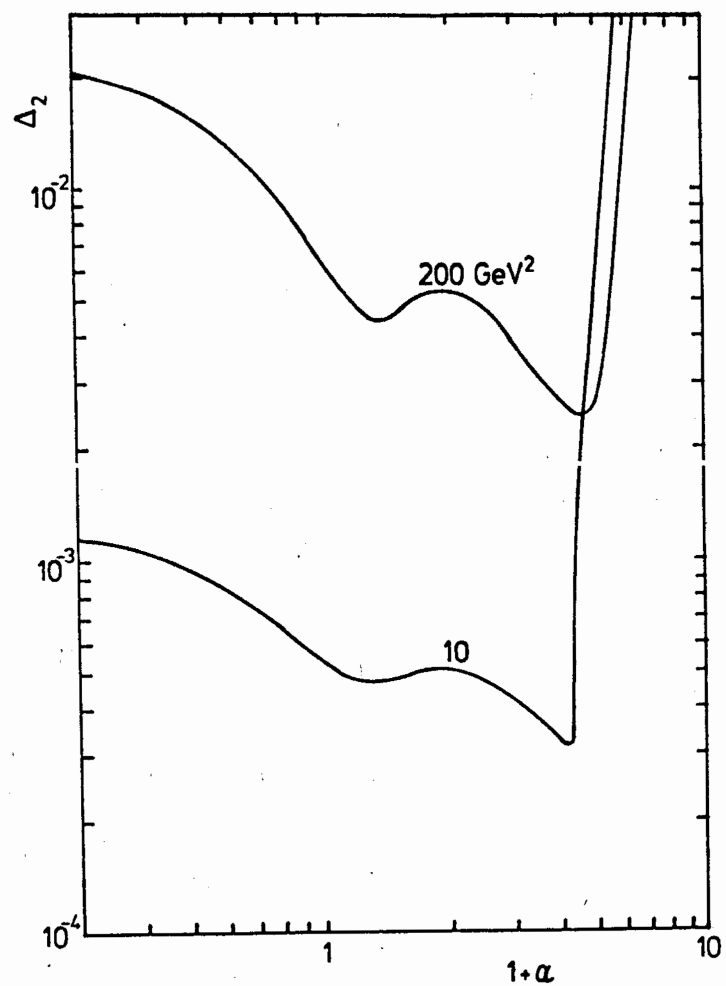

Δ_2
10^{-2}
10^{-3}
10^{-4}
200 GeV^2
10
1
10
$1+\alpha$

Fig. 3

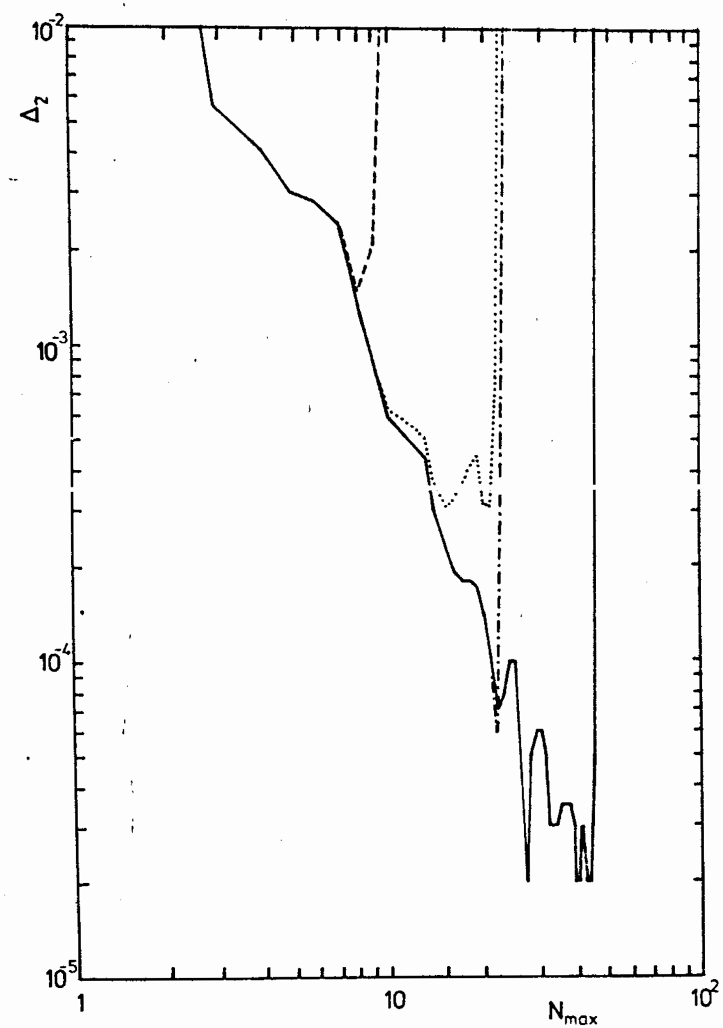

Δ_2
10^{-2}
10^{-3}
10^{-4}
10^{-5}
1
10
10^2
N_{max}

Fig. 4

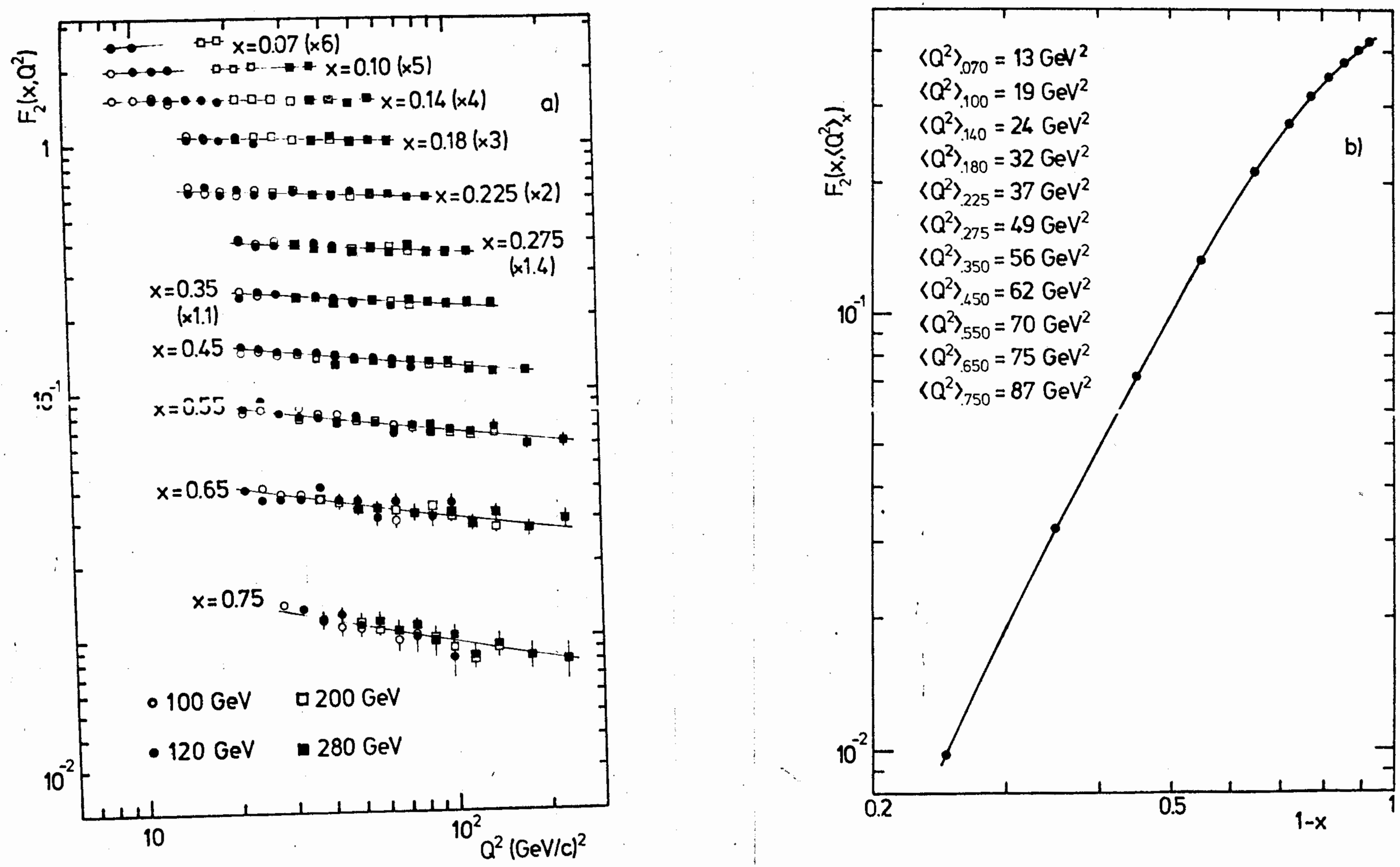
$F_2(x,Q^2)$
x=0.07 (×6)
x=0.10 (×5)
x=0.14 (×4)
x=0.18 (×3)
x=0.225 (×2)
x=0.275 (×1.4)
x=0.35 (×1.1)
x=0.45
x=0.55
x=0.65
x=0.75
a)
100 GeV
120 GeV
200 GeV
280 GeV
1
10^{-1}
10^{-2}
10
10^2
Q^2 (GeV/c)^2
$F_2(x,\langle Q^2\rangle_x)$
$\langle Q^2\rangle_{.070}$ = 13 GeV^2
$\langle Q^2\rangle_{.100}$ = 19 GeV^2
$\langle Q^2\rangle_{.140}$ = 24 GeV^2
$\langle Q^2\rangle_{.180}$ = 32 GeV^2
$\langle Q^2\rangle_{.225}$ = 37 GeV^2
$\langle Q^2\rangle_{.275}$ = 49 GeV^2
$\langle Q^2\rangle_{.350}$ = 56 GeV^2
$\langle Q^2\rangle_{.450}$ = 62 GeV^2
$\langle Q^2\rangle_{.550}$ = 70 GeV^2
$\langle Q^2\rangle_{.650}$ = 75 GeV^2
$\langle Q^2\rangle_{.750}$ = 87 GeV^2
b)
10^{-1}
10^{-2}
0.2
0.5
1
1-x

Fig. 5

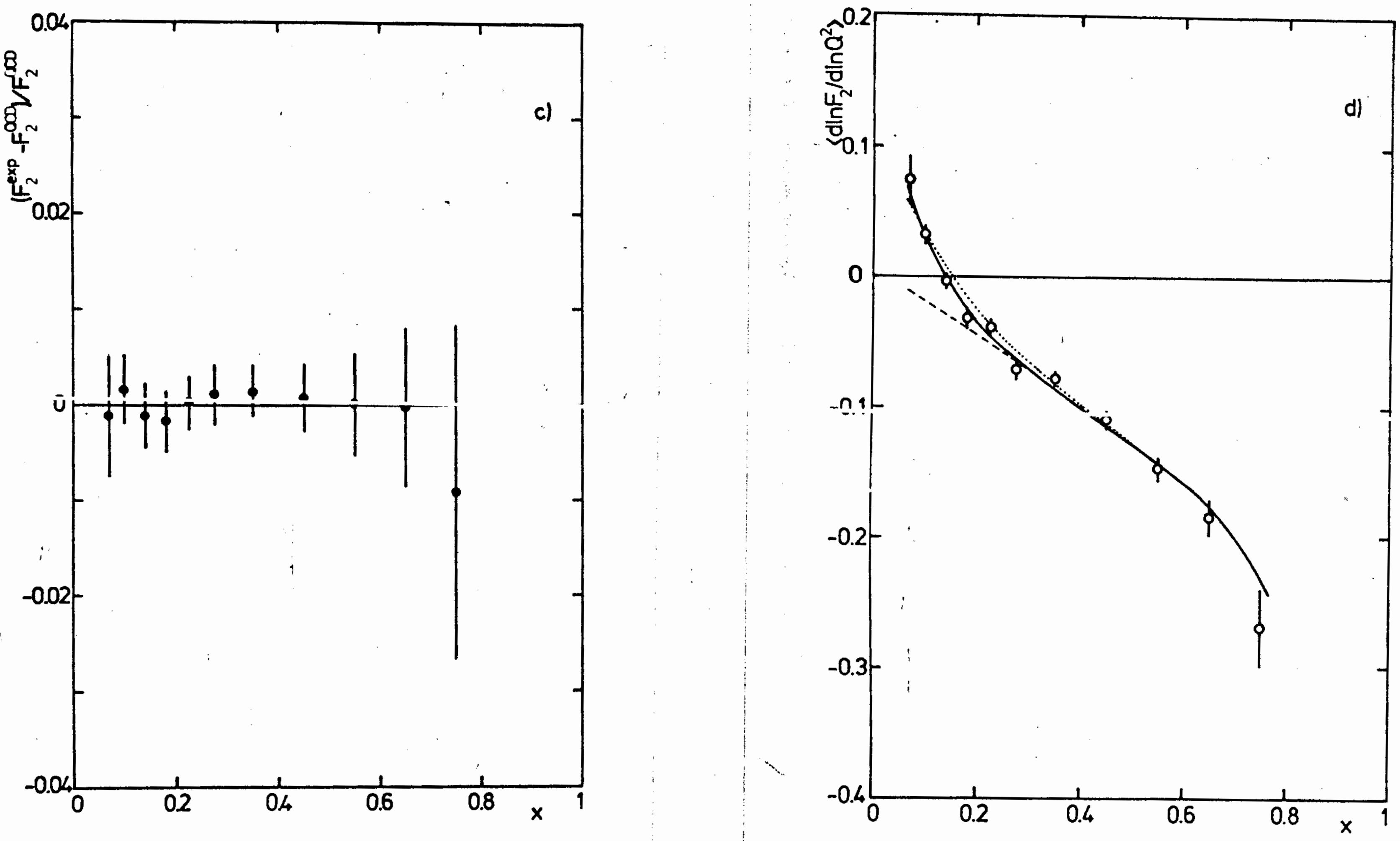

c)
$(F_2^{exp} - F_2^{QCD})/F_2^{QCD}$
0.04
0.02
0
-0.02
-0.04
0
0.2
0.4
0.6
0.8
x
1
d)
$\langle d\ln F_2/d\ln Q^2 \rangle$
0.2
0.1
0
-0.1
-0.2
-0.3
-0.4
0
0.2
0.4
0.6
0.8
x
1

Fig. 5

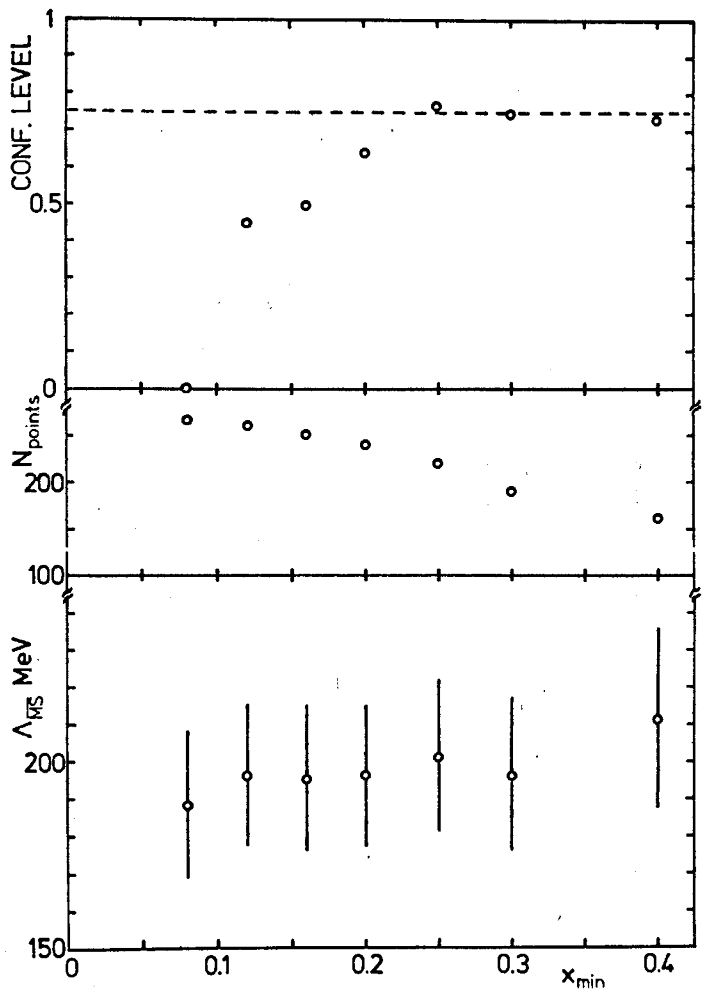
CONF. LEVEL
1
0.5
0
N points
200
100
Λ MS MeV
200
150
0
0.1
0.2
0.3
0.4
x min

Fig. 6

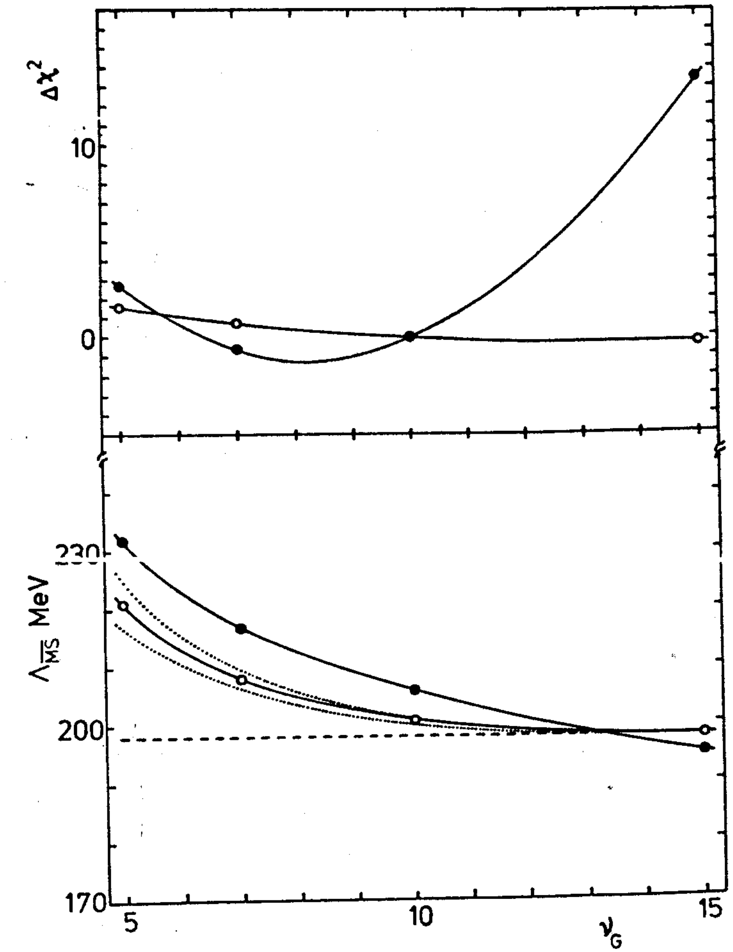
Δχ²
10
0
Λ MS MeV
230
200
170
5
10
15
ν G

Fig. 7

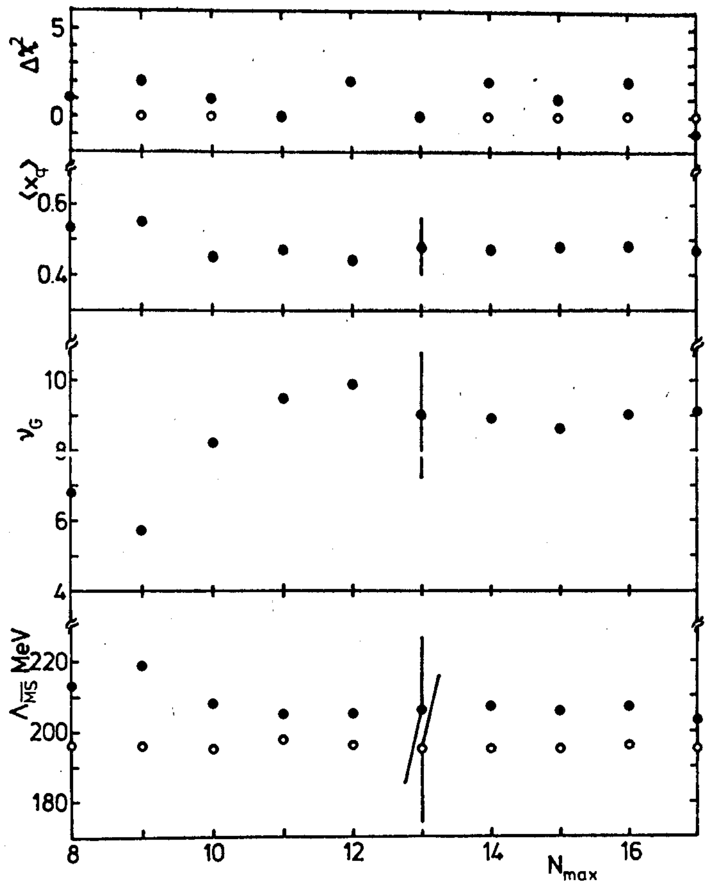

$\Delta\chi^2$
$\langle x_q \rangle$
ν_G
$\Lambda_{\overline{MS}}$ MeV
N_{max}

Fig. 8

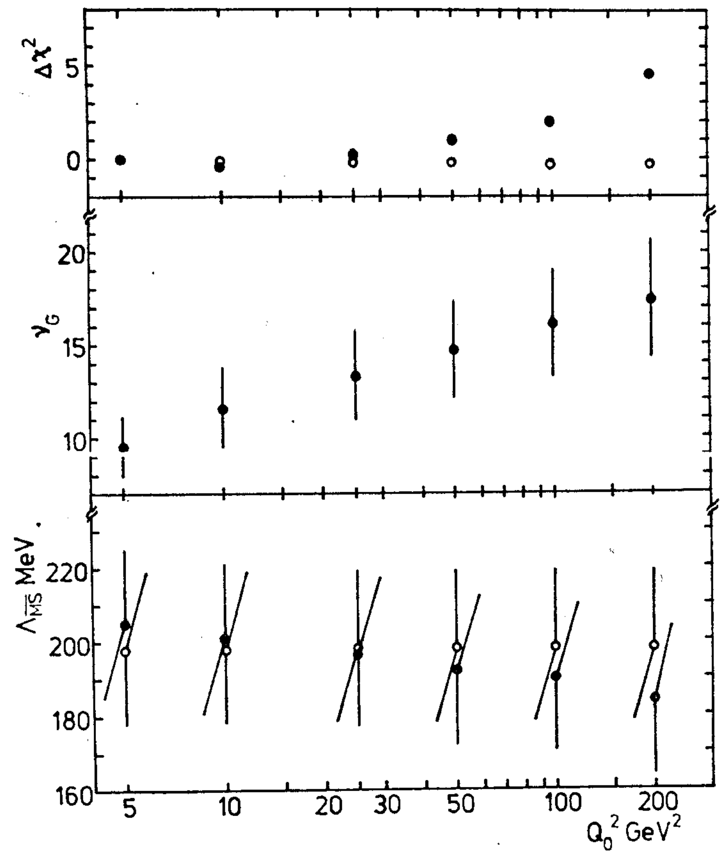

$\Delta\chi^2$
ν_G
$\Lambda_{\overline{MS}}$ MeV
Q_0^2 GeV^2

Fig. 9

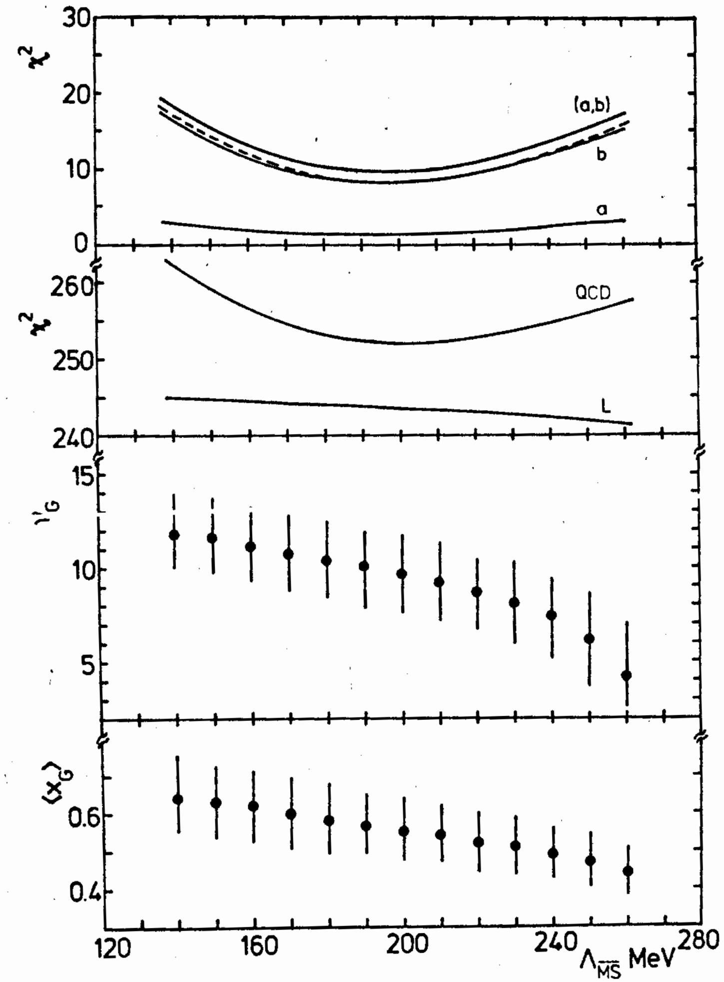

30
20
10
0
260
250
240
15
10
5
0.6
0.4
120
160
200
240
280
(a,b)
b
a
QCD
L
χ^2
ν_G
$\langle x_G \rangle$
$\Lambda_{\overline{MS}}$ MeV

Fig. 10

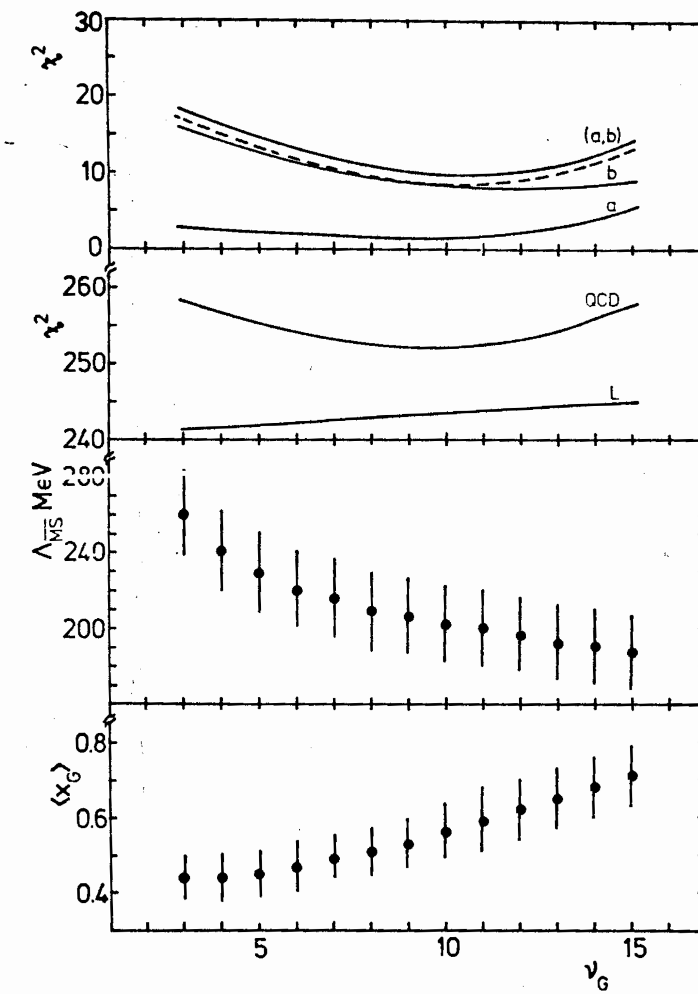

30
20
10
0
260
250
240
280
240
200
0.8
0.6
0.4
5
10
15
(a,b)
b
a
QCD
L
χ^2
$\Lambda_{\overline{MS}}$ MeV
$\langle x_G \rangle$
ν_G

Fig. 11

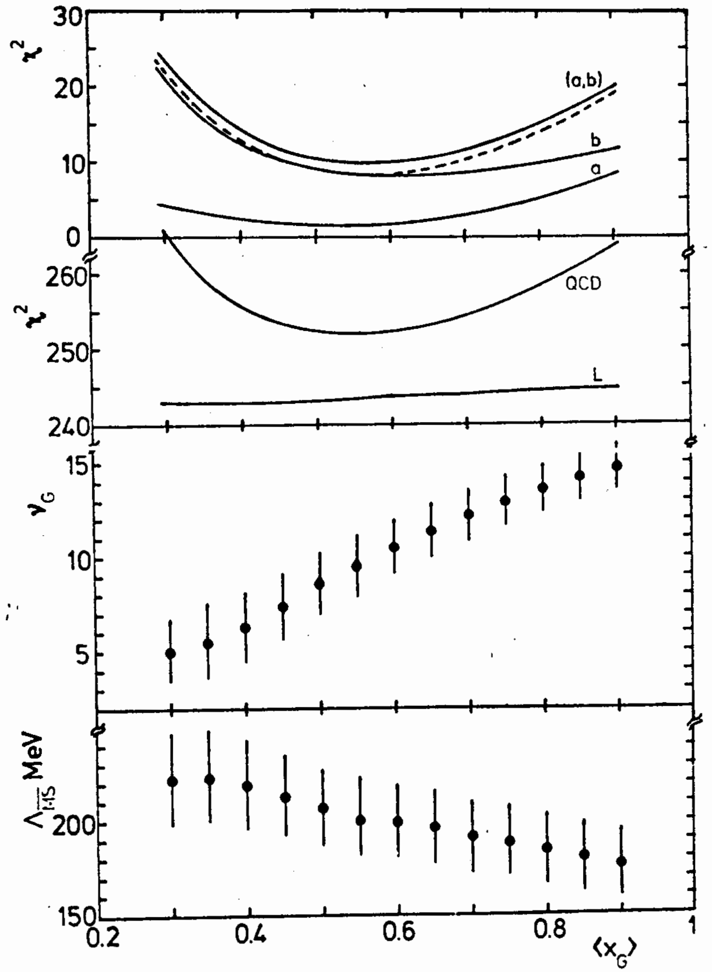

χ^2
(a,b)
b
a
QCD
L
ν_G
$\Lambda_{\overline{MS}}$ MeV
$\langle x_G \rangle$

Fig. 12

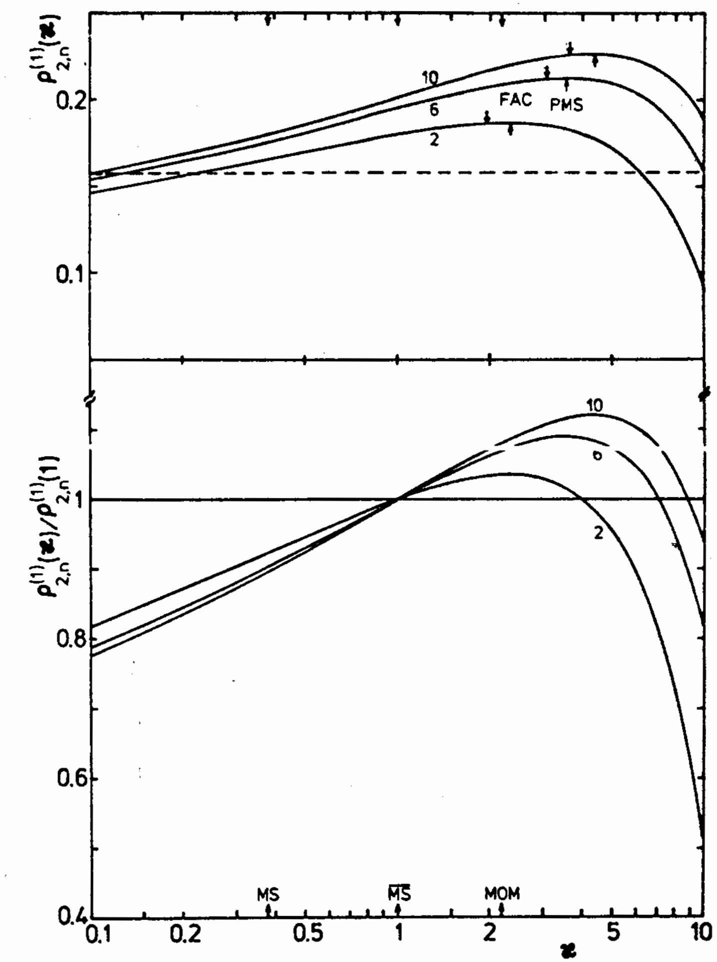

$\rho^{(1)}_{2,n}(\varkappa)$
10
6
2
FAC
PMS
$\rho^{(1)}_{2,n}(\varkappa)/\rho^{(1)}_{2,n}(1)$
MS
$\overline{MS}$
MOM
$\varkappa$

Fig. 13

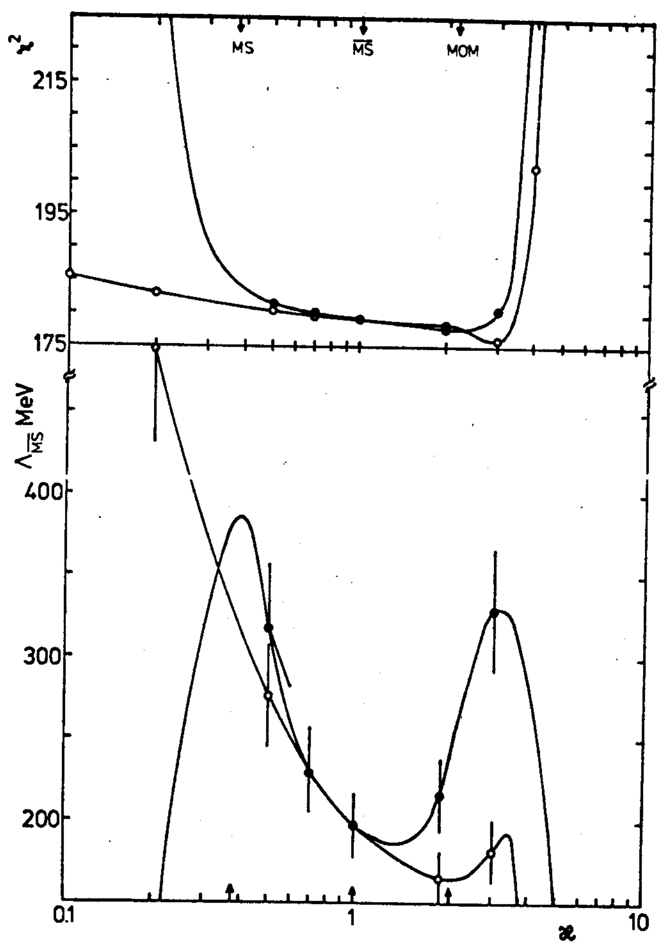
χ^2
215
195
175
MS
$\overline{MS}$
MOM
$\Lambda_{\overline{MS}}$ MeV
400
300
200
0.1
1
10
$\varkappa$

Fig. 14

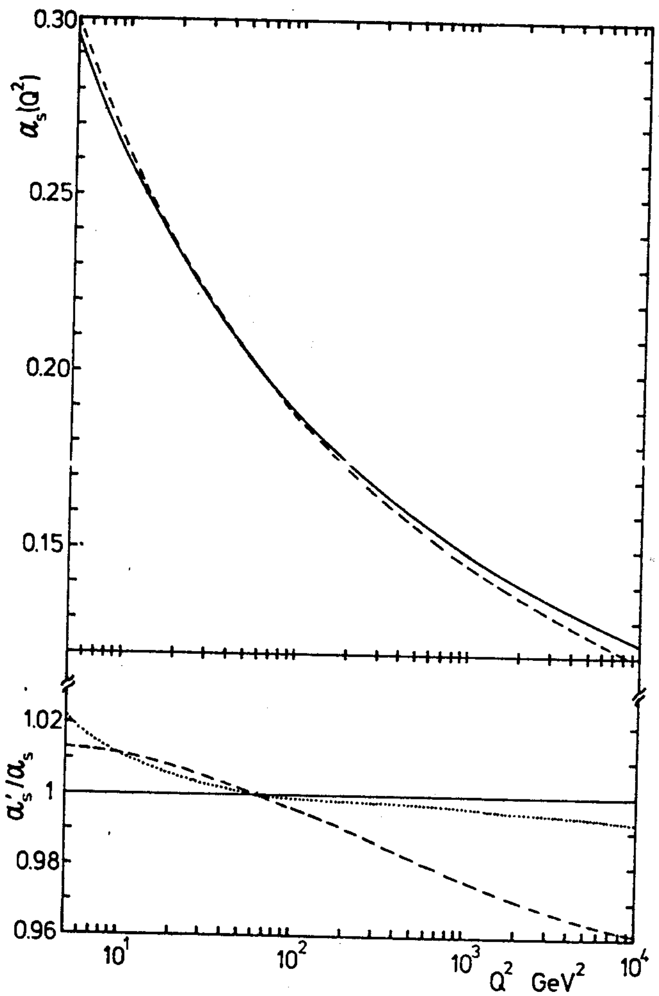
$\alpha_s(Q^2)$
0.30
0.25
0.20
0.15
α_s'/α_s
1.02
1
0.98
0.96
10^1
10^2
10^3
Q^2 GeV^2
10^4

Fig. 15

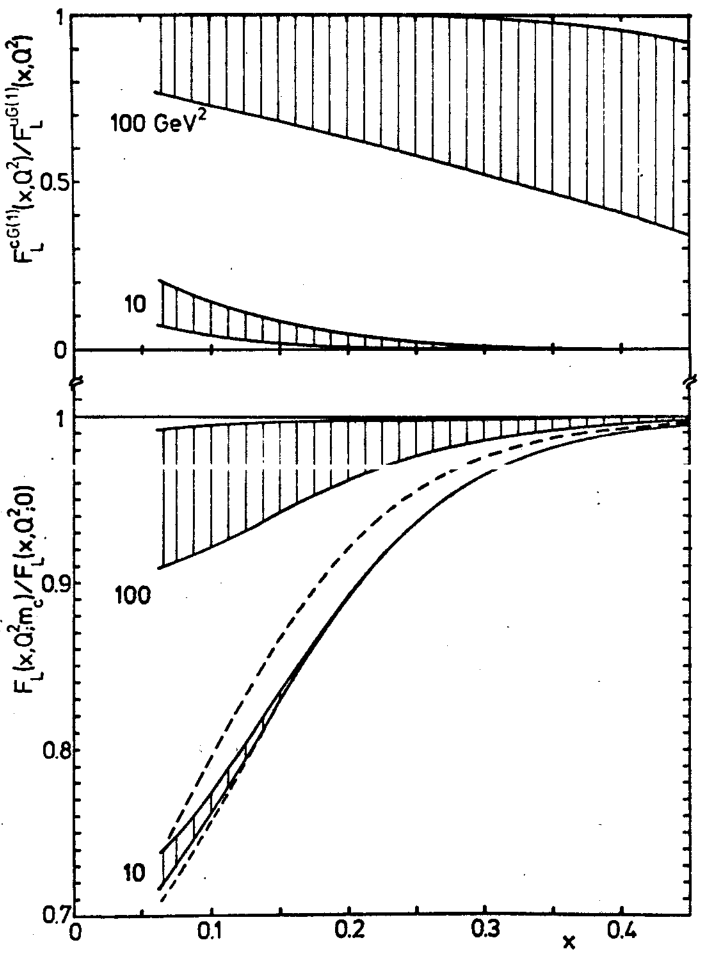

$F_L^{cG(1)}(x,Q^2)/F_L^{uG(1)}(x,Q^2)$
100 GeV^2
10
$F_L(x,Q^2;m_c)/F_L(x,Q^2;0)$
100
10
x

Fig. 16

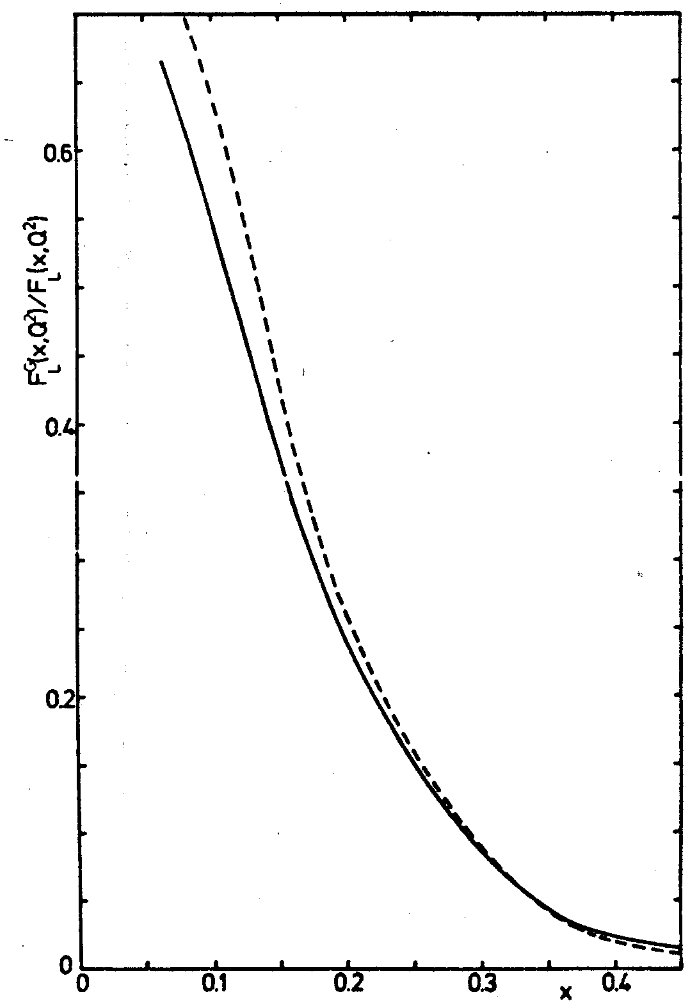

$F_L^c(x,Q^2)/F_L(x,Q^2)$
x

Fig. 17

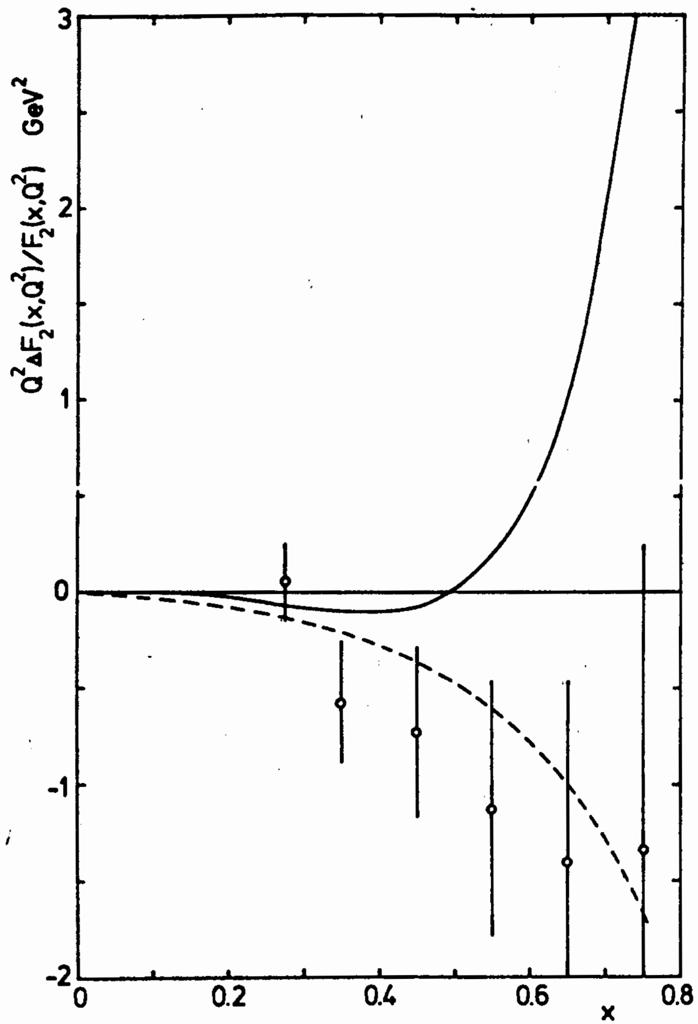

$Q^2\Delta F_2(x,Q^2)/F_2(x,Q^2)$ GeV^2
3
2
1
0
-1
-2
0
0.2
0.4
0.6
0.8
x

Fig. 18

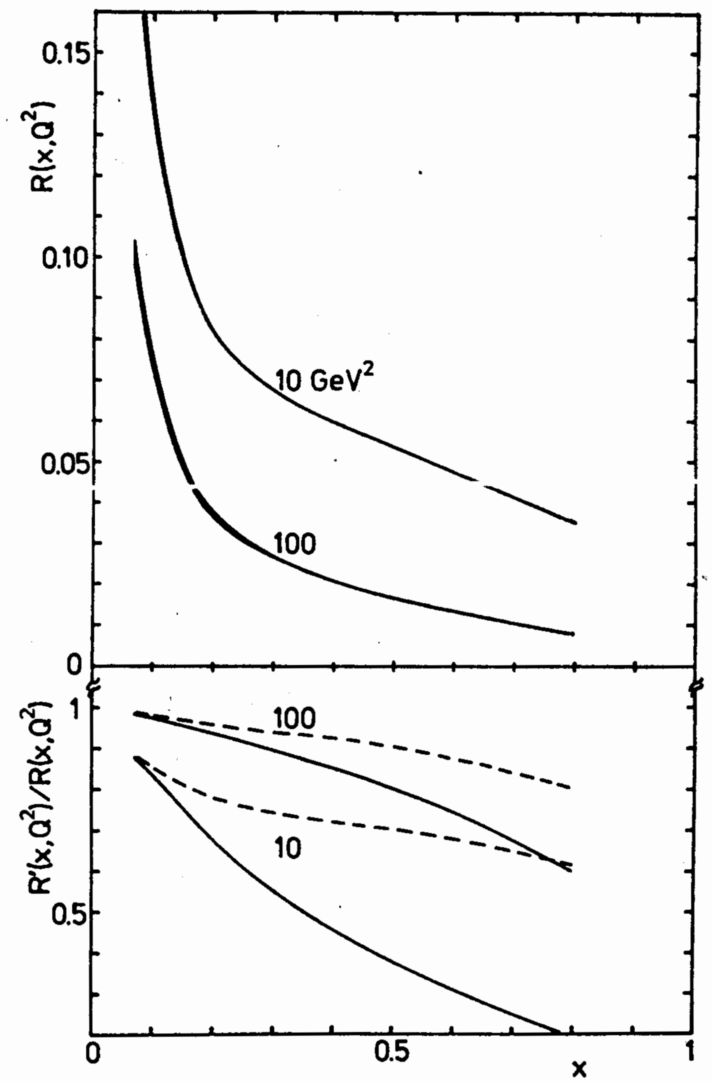

$R(x,Q^2)$
0.15
0.10
0.05
0
10 GeV^2
100
$R'(x,Q^2)/R(x,Q^2)$
1
0.5
100
10
0
0.5
1
x

Fig. 19

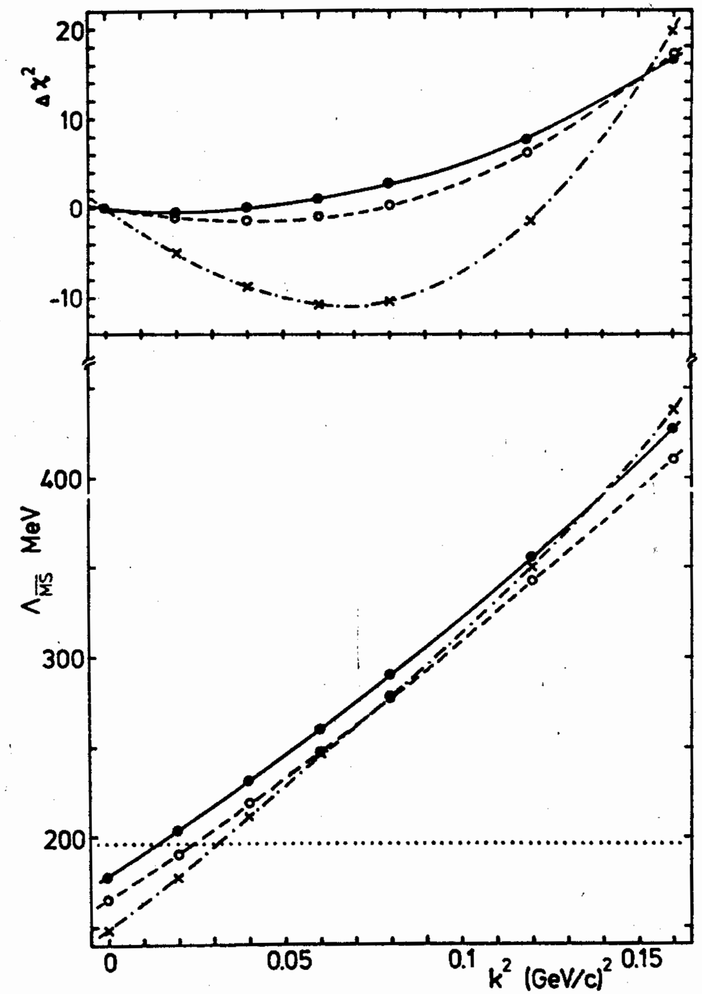

20
10
0
-10
$\Delta\chi^2$
400
300
200
$\Lambda_{\overline{MS}}$ MeV
0
0.05
0.1
0.15
k^2 (GeV/c)^2

Fig. 20

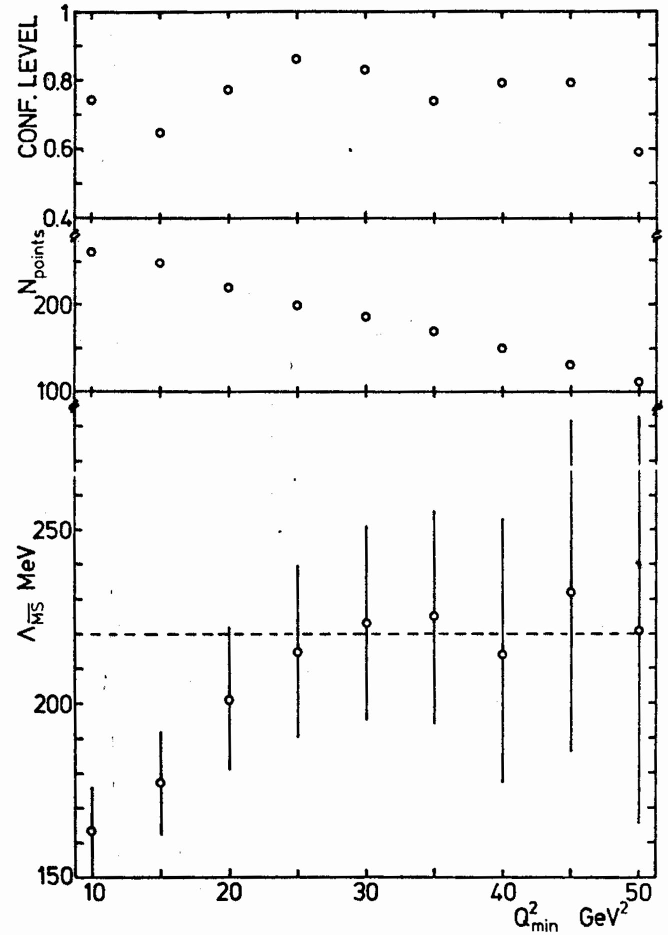

CONF. LEVEL
1
0.8
0.6
0.4
N_{points}
200
100
$\Lambda_{\overline{MS}}$ MeV
250
200
150
10
20
30
40
50
Q^2_{min} GeV^2

Fig. 21